A Numerical Study of the Coastal Cyclogenesis in GALE IOP 2: Sensitivity to PBL Parameterizations

TEDDY HOLT*

Department of Marine, Earth and Atmospheric Sciences, North Carolina State University, Raleigh, North Carolina

SIMON CHANG

Atmospheric Physics Branch, Naval Research Laboratory, Washington, D.C.

SETHU RAMAN

Department of Marine, Earth and Atmospheric Sciences, North Carolina State University, Raleigh, North Carolina

ABSTRACT

The effects of different parameterizations of the boundary layer on atmospheric mesoscale structure are tested in a three-dimensional limited area weather forecast model. Model simulations are performed for three model designs: 1) a 10-layer model with a 1-layer bulk planetary boundary layer (PBL), 2) a 16-layer model with a 1-layer bulk parameterization of the surface layer but a mixing-length PBL parameterization, and 3) a 16-layer model with a surface energy budget, Monin–Obukhov similarity surface layer and a PBL parameterization based on turbulent kinetic energy (TKE) closure. Model simulations are compared to Genesis of Atlantic Lows Experiment (GALE) data, including aircraft observations, for the period 25–26 January 1986 during Intensive Observing Period (IOP) 2 in which coastal frontogenesis and cyclogenesis were prominent.

Results indicate that for mean and perturbation mesoscale structure of winds, temperature and moisture in areas of more complex atmospheric processes such as the Appalachian Mountains, coastal and Gulf Stream regions, the improved TKE boundary layer parameterization provides more accurate as well as realistic forecasts. An increase in vertical resolution in the boundary layer alone does not provide substantial improvement if turbulent boundary layer processes are not properly accounted for in the PBL parameterization. Even with increased boundary layer resolution, model simulations with an inadequate parameterization, particularly in regions of rapidly varying atmospheric stability, show poorer forecasts of vertical and horizontal mesoscale structure. For this one case study, the simple 10-layer constant depth bulk PBL model does well in forecasting wind, temperature and moisture fields. Results comparable to the more complex TKE parameterization model are obtained for relatively homogeneous conditions. The 10-layer model, however, lacks the vertical resolution or proper PBL parameterization to resolve more detailed structure evident in vertical sounding profiles along the developing coastal front.

Skill scores indicate little sensitivity in the larger mesoscale structure to changes in PBL parameterization. Similar S_1 scores and root-mean-square (rms) errors for sea level pressure fields are obtained for each of the three model designs; however, surface latent and sensible heat fluxes are important in the development of the coastal front system with model simulations without surface fluxes showing no coastal low pressure system and reduced precipitation. Comparison to aircraft observations obtained in the vicinity of the Gulf Stream approximately 5–6 hours after the frontal passage supports the conclusions drawn from model simulations with a TKE PBL parameterization of a relatively deep (600 m), well-mixed, postfrontal marine boundary layer.

1. Introduction

With the fact that much significant weather, particularly precipitation, occurs on the mesoscale (Orlanski 1975), a great deal of attention has been focused recently on regional or limited area numerical weather prediction (NWP) models which have grid sizes and domains theoretically capable of capturing such events. Recent development in operational and research limited area NWP models has been reviewed by Anthes (1983). One of the principal difficulties in the incorporation of limited area models, as discussed by Anthes (1983), is the "increase in importance of and difficulty in modeling diabatic, topographic, and surface effects." These effects become increasingly more important in regions of, for example, marked horizontal surface roughness and/or temperature changes such as coastal regions, marked topography changes such as the Appalachian Mountains, and regions of strong low-level heating and air mass modification such as the Gulf

---

* Present affiliation: Dept. of Meteorology, Naval Postgraduate School, Monterey, California.

Corresponding author address: Dr. Simon Chang, Department of the Navy, Naval Research Laboratory, Atmospheric Physics Branch, Code 4110, Washington, DC 20375-5000.

Stream regions. Thus, improved physical parameterizations to handle these effects properly in a model should be included.

Recent studies of coastal cyclogenesis and frontogenesis have emphasized the importance of a variety of physical processes. Research on the well-documented President's Day storm of 18–19 February 1979 by Bosart (1981), Bosart and Lin (1984) and Uccellini et al. (1985) showed the importance of sensible heat transport and latent heat release, upper-level jet streaks and coastal frontogenesis in the evolution of the coastal cyclone. In a numerical case study of East Asian coastal cyclogenesis, Chen and Dell'Osso (1987) emphasized the importance of latent heat feedback in deepening the coastal cyclone, with sensible heating less essential. Ballentine's (1980) numerical study of New England coastal frontogenesis showed that upper level synoptic scale forcing was a necessary but insufficient condition for strong coastal front development while strong surface heat fluxes from the ocean were mainly responsible for convergence at the coast. The importance of the coastline curvature in enhancing coastal front development was examined by Bosart (1975). Marks and Austin (1979) showed the coastal front to be a relatively shallow, low-level phenomenon occurring ahead of the surface cyclone and synoptic scale warm front with precipitation resulting primarily from a local intensification of the large scale circulation.

The purpose of this paper is to examine the effectiveness of differing planetary boundary layer (PBL) parameterizations in a three-dimensional (3-D) limited area model using Genesis of Atlantic Lows Experiment (GALE) data for 1200 UTC 25 January to 1800 UTC 26 January 1986 during Intensive Observing Period (IOP) 2. [For more information on the GALE field program phase, see Dirks et al. (1988) or Raman and Riordan (1988).] The emphasis here is on improvements in mesoscale forecasts, particularly features such as the sea level pressure (SLP) fields, coastal front temperature gradient, wind shift line and low-level jet, in the area of more complex atmospheric processes as mentioned above. Inherent in the comparison of increasingly more complex multilevel PBL parameterizations is the need to examine the effects of increased vertical model resolution. An increase in vertical resolution in a multilevel model is advantageous when the complexity of the parameterizations of the physical processes increases, because of the need to properly resolve these processes. Three PBL parameterizations are considered here and are chosen specifically to examine the importance of the physical PBL parameterization versus increased vertical model resolution.

In section 2 the experiment design for the case study is presented. Included is a brief description of the 3-D limited area model along with the three PBL parameterizations chosen. The detailed synoptic situation of the case study during GALE IOP 2 is described in section 3. Results from the 3-D limited area model are presented in section 4 in terms of mesoscale structure, cross-sectional analysis and statistical analysis. Mesoscale structure provides a subjective comparison of the location, movement and intensification of the coastal front. Statistical analysis of mesoscale model results provides a more objective, though general, overview of the accuracy of a forecast. Typical statistical parameters used to show a model's skill on the larger meso-α (200–2000 km) horizontal scale include root-mean-square (rms) errors and S_1 scores. Conclusions drawn from statistical analysis, however, are often limited to the larger scale. Atmospheric structure on the smaller meso-β (20–200 km) horizontal scale can be studied better both temporally and spatially by detailed analysis of cross sections. Both statistical and cross section analysis are used in this study to evaluate the forecast skills on the meso-α and meso-β scales. Also discussed in section 4 are the sensitivity of model results to surface fluxes and the comparison to available aircraft data.

2. Experiment design

a. Brief model description

The Naval Research Laboratory (NRL) limited area dynamic numerical weather prediction model is a 3-D model incorporating various processes affecting both small scale and larger scale phenomena. Provided here is only a brief model review. Madala et al. (1987) and Chang et al. (1989) provide a more extensive model description.

The seven governing primitive equations are written in surface pressure weighted form and include equations for u- and v-momentum, temperature, moisture continuity, surface pressure tendency, hydrostatic equilibrium and mass continuity. The model has 91 × 51 horizontal grid points with 0.5 degree resolution in the domain of 25°–45°N, 100°–60°W.

The vertical coordinate is the terrain following σ, defined as the ratio of pressure p to surface pressure p_s. The horizontal grid network is the C-grid (Arakawa and Lamb 1977). On this grid, temperature (T), geopotential (ϕ), humidity (q) and σ are computed at mass points (i, j) while east–west velocity u is computed at the midpoint of mass points along the x-axis and north–south component v is computed at midpoints along the y-axis. Vertical velocity $\dot{\sigma}$, defined as $d\sigma/dt$, is evaluated at half levels in the vertical between those given in Table 1.

The basic dataset used in the initialization is the NMC/RAFS (National Meteorological Center/Regional Analysis and Forecasting System) 2.5 degree hemispheric analyses (without enhanced GALE data) interpolated by cubic polynomial to half degree resolution. A variety of initialization schemes were tested in the 3-D model including uninitialized and balanced ones. The initialization chosen was nondivergent winds on pressure surfaces and observed temperatures and moistures. This was found to produce the best forecasts

TABLE 1. Vertical model (σ) levels.

Model level K	Model			
	M10		MB16 (and EE16)	
	σ	p (mb) (approx)	σ	p (mb) (approx)
1	0.05	50	0.05	50
2	0.15	150	0.15	150
3	0.25	250	0.25	250
4	0.35	350	0.35	350
5	0.45	450	0.45	450
6	0.55	550	0.55	550
7	0.65	650	0.65	650
8	0.75	750	0.75	750
9	0.85	850	0.82	820
10	0.95	950	0.86	860
11			0.90	900
12			0.935	935
13			0.96	960
14			0.9775	977
15			0.99	990
16			0.9975	997

in previous model simulations (Chang et al. 1989; Brehme 1987).

Proper specification of lateral boundary conditions in a limited area model is paramount to accurate model forecasts. In limited area models, improper handling of boundary conditions can often offset any advantages gained by increased horizontal resolution. Numerous schemes exist to determine lateral boundary conditions including fixed, time-dependent, sponge and relaxation (or nudging) (Perkey and Kreitzberg 1976; Davies and Turner 1977). Both sponge and relaxation schemes have been tested in the NRL 3-D model (Chang et al. 1989). The preferred relaxation scheme, in which values within five grid points were nudged toward the NMC large scale analyses, is used here:

$$\frac{\delta X}{\delta t} = (1 - \alpha)\left(\frac{\delta X}{\delta t}\right)m + \gamma(X_0 - X) \qquad (1)$$

where X represents the dependent variables, $(\delta X/\delta t)_m$ represents model computed tendencies, γ is the relaxation parameter (equal here to Coriolis parameter f), α is the weighting parameter and is a linear function of distance from the lateral boundaries, and X_0 represents large scale values. Thus, boundary conditions are updated every 12 hours using NMC large scale analyses and the damping and relaxation (nudging) scheme of (1).

Parameterized physics included in the model are convective and nonconvective precipitation, dry convective adjustment and a planetary boundary layer parameterization. Atmospheric radiation is not considered because of the relatively short model integration time (30 h). Convective precipitation is parameterized using a modified Kuo scheme (Kuo 1974; Anthes 1977). When low-level moisture convergence reaches

a certain threshold in a conditionally unstable environment, convective precipitation occurs in the model. No subgrid scale moisture convergence is considered. Nonconvective precipitation occurs in the model when saturation is reached on the resolvable scale. Excess moisture, computed from the Clausius–Clapeyron equation, precipitates into lower model layers and evaporates or falls to the surface. A dry convective adjustment, which conserves total static energy, is included in the model above the PBL to neutralize superadiabatic lapse rates.

b. Model design

The three model designs considered here are a simple 10-layer model (M10), and two 16-layer models (MB16 and EE16). The model dynamics and basic equations are the same for each. Only vertical model resolution and the PBL parameterizations are changed. Differences in the structure of the three models are given below.

M10—The simplest model design has 10 levels in the vertical of equal σ thickness. The boundary layer is contained in the lowest level and is parameterized by the bulk aerodynamic (drag coefficient) method. Surface stress in the x and y directions is given by

$$\tau_x = \rho u^{*2} \frac{U}{\bar{V}}$$

$$\tau_y = \rho u^{*2} \frac{V}{\bar{V}} \qquad (2)$$

where $\bar{V}$ is the mean resultant wind. Friction velocity u^* is computed as

$$u^* = (C_D \bar{V}^2)^{1/2} \qquad (3)$$

where the drag coefficient C_D for momentum is taken to be

$$C_D = \begin{cases} 2.5 \times 10^{-3} & \text{over land} \\ 1.0 \times 10^{-3} & \text{over ocean.} \end{cases} \qquad (4)$$

Sensible and latent heat exchange with the surface is achieved through

$$(\overline{w\theta})_0 = -u^* T^*$$

$$(\overline{wq})_0 = -u^* q^* \qquad (5)$$

where the temperature (T^*) and moisture (q^*) scaling parameters are defined as

$$T^* = C_E \bar{V} \frac{(\Theta - \Theta_s)}{u^*}$$

$$q^* = C_E \bar{V} \frac{(q - q_s)}{u^*} \qquad (6)$$

where the subscript s represents near-surface values and

the drag coefficient C_E for heat and moisture is defined as

$$C_E = \begin{cases} 0. & \text{over land} \\ 2.0 \times 10^{-3} & \text{over ocean.} \end{cases} \quad (7)$$

The simple bulk model is essentially the same as the model of Chang et al. (1989) with no sensible or latent heat flux allowed over land ($C_E = 0$) to simplify the comparison of results.

MB16—The next model considered has 16 levels in the vertical with varying resolution in the boundary layer (see Table 1). MB16 (and EE16) both have seven levels in the lowest 150 mb compared to one in the 10-layer model. The lowest model level represents the surface layer and the same bulk aerodynamic method is used as in M10. The PBL parameterization used in MB16 is a modification of the first order mixing-length (*l*) approach of Blackadar (1962):

$$l = kz/(1 + kz/\lambda) \quad (8)$$

where k is von Kármán's constant and z is height with λ taken to be 50 m. For Blackadar's original formulation [$\lambda = 2.7 \times 10^{-4} |G|/|f|$], where f is the Coriolis parameter, this is equivalent to assuming the geostrophic wind $G = 15.5$ m s^{-1} for midlatitudes (see Holt and Raman 1988).

EE16—The most complex model considered in terms of the PBL parameterization uses the turbulent kinetic energy (TKE) $E - \varepsilon$ closure with the constants (*c*) of Detering and Etling (1985). Prognostic equations for turbulent kinetic energy (E) and energy dissipation (ε) are incorporated as (see Gerber et al. 1989)

$$\frac{\partial E}{\partial t} = -\overline{uw}\,\frac{\partial U}{\partial z} - \overline{vw}\,\frac{\partial V}{\partial z} + \frac{g}{\Theta}\,\overline{w\theta}$$
$$- \frac{\partial}{\partial z}\left(\overline{wE} + \frac{\overline{pw}}{\rho}\right) - \varepsilon \quad (9)$$

$$\frac{\partial \varepsilon}{\partial t} = c_1 \frac{\varepsilon}{E}\left(-\overline{uw}\,\frac{\partial U}{\partial z} - \overline{vw}\,\frac{\partial V}{\partial z} + \frac{g}{\Theta}\,\overline{w\theta}\right)$$
$$- c_2 \frac{\varepsilon^2}{E} + c_3 \frac{\partial}{\partial z}\left(K_m \frac{\partial \varepsilon}{\partial z}\right) \quad (10)$$

where $\overline{uw}$, $\overline{vw}$ are turbulent fluxes of momentum, ρ is density, p is fluctuating pressure and K_m is the eddy viscosity coefficient. The first two terms on the right-hand side (rhs) of (9) represent shear production, the third represents buoyancy production and the fourth turbulent transport. The three terms on the rhs of (10) represent the production, destruction and transport of energy, respectively.

In addition to the improved parameterization of the PBL, model EE16 also differs from the other two models in the treatment of the surface boundary layer. At the surface, the ground temperature T_g is predicted by a soil slab model (Blackadar 1976) while the surface

layer is parameterized by the Monin–Obukhov (M-O) similarity relations (Businger et al. 1971).

The soil slab model incorporated in EE16 predicts ground surface temperature T_g based on the surface energy equation (Chang 1979)

$$\frac{\partial T_g}{\partial t} = RC_g^{-1} + \omega(T_m - T_g) + \rho C_p(\overline{\omega\theta})_0 C_g^{-1} \quad (11)$$

where R is net radiation, C_g is heat capacity per unit area of soil slab, ω is the inverse of the time scale for heat conduction in the soil ($2\pi/1$ day), T_m is deep soil temperature, ρC_p is for air and $(\overline{\omega\theta})_0$ is defined in (5). The terms on the right-hand side of (11) represent net radiation, soil heat flux and surface heat flux. Net radiation R is the sum of incoming solar radiation absorbed at the surface I_s, atmospheric longwave backscattering radiation I_L and outgoing longwave surface radiation O_L. Incoming solar radiation is estimated as

$$I_s = S \cos Z(1 - A)b^{\sec Z} \quad (12)$$

where S is the solar constant, Z is solar zenith angle, b is atmospheric turbidity, which is a function of precipitation rate, and A is surface albedo obtained from land use data over the model domain from the Fleet Numerical Ocean Center (FNOC).

Water vapor is ignored in the relationship for net longwave radiation computed using Brunt's equation (Seller 1965):

$$I_L - O_L = -\epsilon(1 - 0.61)\beta T_g^4 \quad (13)$$

where ϵ is soil emissivity (0.7) and β is the Stefan–Boltzmann constant. Heat capacity of the soil slab C_g is approximated as an 80 m deep air layer (Chang 1979).

The surface boundary layer is parameterized based on similarity theory (Monin and Yaglom 1971):

$$\frac{kz}{u^*}\frac{\partial U}{\partial z} = \phi_m(z/L)$$
$$\frac{kz}{\theta^*}\frac{\partial \Theta}{\partial z} = \phi_h(z/L)$$
$$\frac{kz}{q^*}\frac{\partial q}{\partial z} = \phi_n(z/L) \quad (14)$$

where the nondimensional stability parameters ϕ_m and ϕ_h for momentum and heat are functions of the Monin–Obukhov length L (Businger et al. 1971). Roughness length z_0 was a function of terrain heights over land and was calculated over water from Charnock's relation:

$$z_0 = 0.0144u^{*2}/g. \quad (15)$$

The SST distribution was obtained from the climatological 1-degree resolution mean SST values for January given by Reynolds (1982). Initial ground temperature was estimated as a sinusoidal function of solar hour angle, latitude and initial air temperature

TABLE 2. Model characteristics.

	Model		
	M10	MB16	EE16
Vertical levels	10	16	16
Surface boundary layer parameterization	Bulk aerodynamic	Bulk aerodynamic	M–O similarity
SST	Climatology	Climatology	Climatology
Ground surface temperature	Constant	Constant	Surface energy budget
PBL parameterization	Assumed to be well mixed	Mixing length	TKE closure

at the lowest model level. Topography used in the 3-D model was derived from the United States Navy global 10-minute elevation data. Characteristics of each model are summarized in Table 2.

3. Genesis of Atlantic Lows Experiment (GALE): IOP-2

Figure 1 shows the initial fields at 1200 UTC 25 January used in the 30-hour model simulations. Given are SLP, surface water vapor mixing ratio and 850 and 500 mb pressure fields obtained from the NMC/RAFS interpolated data. Prior to 1200 UTC 25 January, cold

air damming had already occurred near the Appalachian Mountains and the shallow coastal front was forming (0800 UTC 25 January)-parallel to the coast near Cape Hatteras, North Carolina. The dashed line in the SLP field of Fig. 1 just offshore of North Carolina representing the coastal front at 1200 UTC was based on high resolution GALE PAM, ship and buoy data (Fig. 2). The NMC analysis hints at a coastal front, but it was not adequately resolved.

Further west at 1200 UTC 25 January, a frontal wave extended through the Midwest to the surface cyclone in extreme southeastern Texas, which eventually became the major cyclone that moved up the East Coast
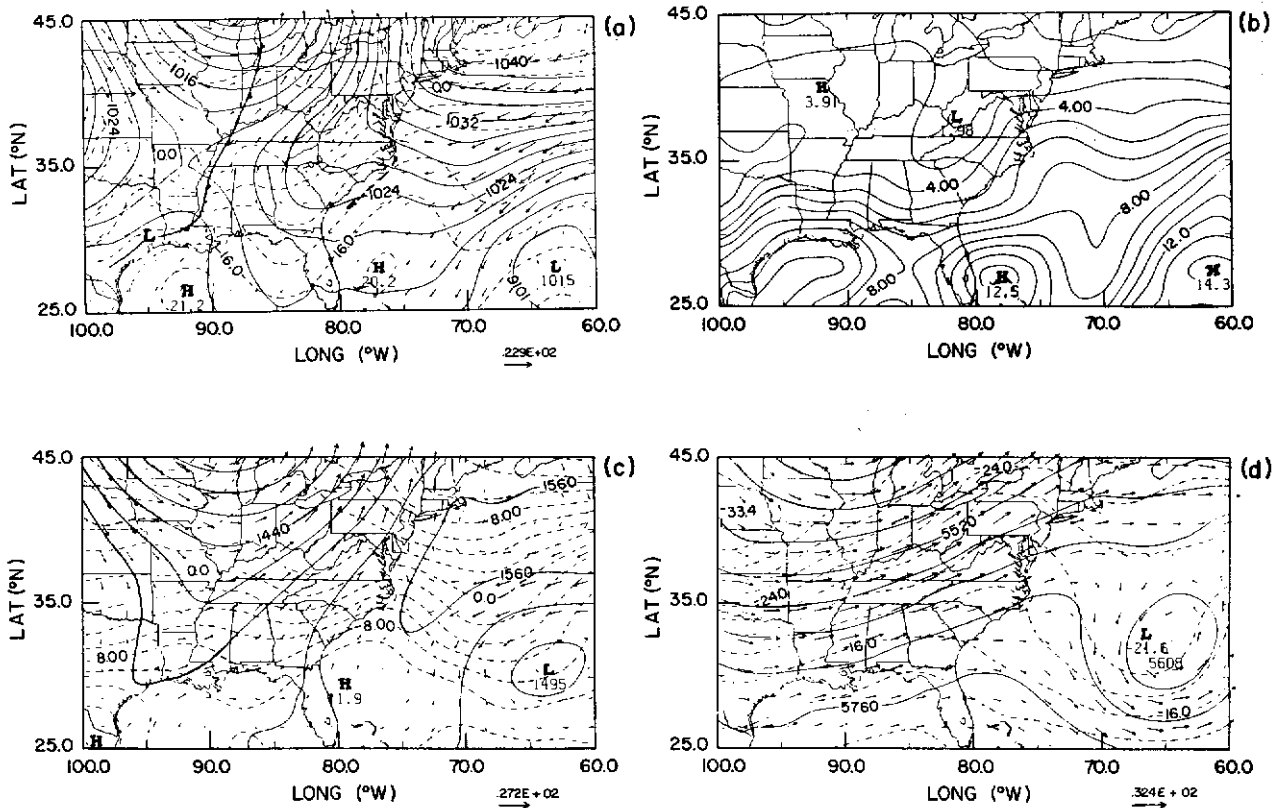

FIG. 1. Initial NMC/RAFS analyses at 1200 UTC 25 January 1986 of (a) sea level pressure (solid lines, mb), surface winds (vectors, m s^{-1}) and temperature (dashed lines, C); (b) surface water vapor mixing ratio (g kg^{-1}); (c) 850 mb winds, temperature and geopotential (solid lines, m) and (d) 500 mb winds, temperature and geopotential. Maximum wind vector (m s^{-1}) is indicated at the lower right for each level.
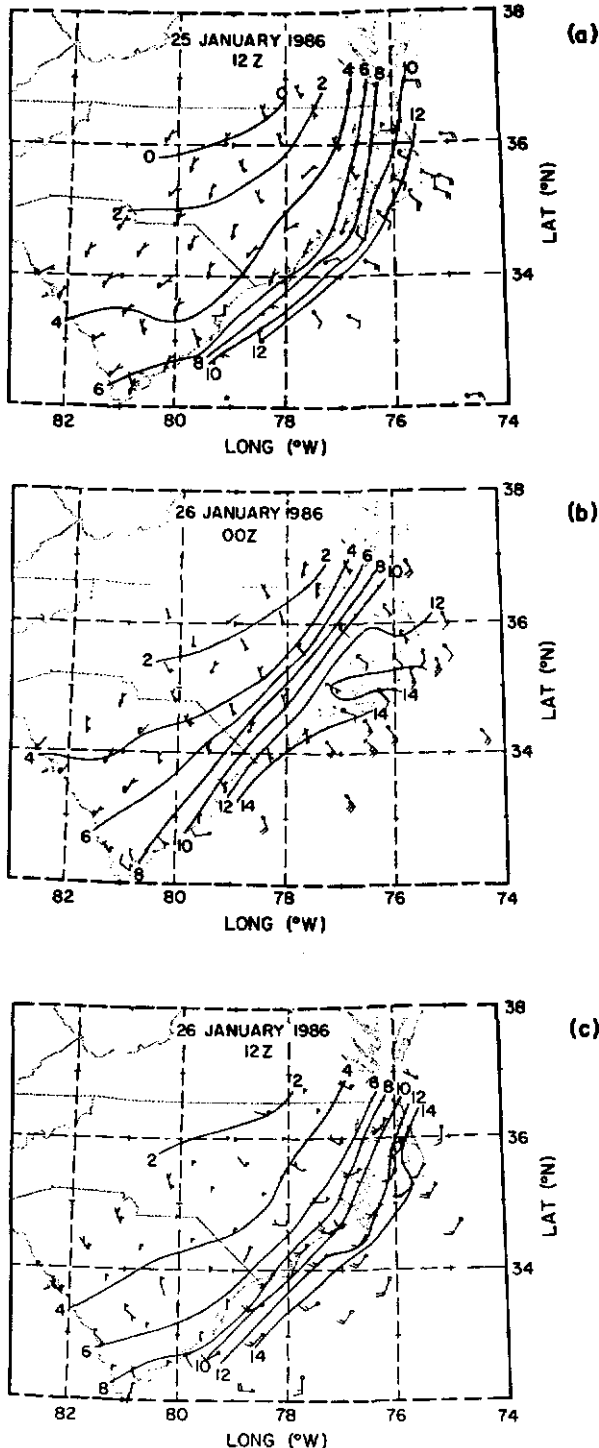
FIG. 2. Surface temperature (solid lines, C) and winds (barbs, knots) from PAM, ship and buoy data for (a) 1200 UTC 25 January, (b) 0000 UTC 26 January and (c) 1200 UTC 26 January.

on 27 January. At 850 mb, significant warm advection over the GALE area accompanied the coastal frontogenesis. By 0000 UTC 26 January, the main low pres-

sure system in Texas had progressed to the Alabama Gulf coast with a quasi-stationary front stretching across Florida. The coastal front was now firmly established along the East Coast and was readily identified in the PAM network (Fig. 2b). The warm advection at 850 mb, however, had shifted and was now confined to regions north of South Carolina with the upper-level trough at 500 mb still situated over the central United States. The surface mesoscale analysis indicated a weak subsynoptic scale low pressure center had formed on the coastal front off the coast of Georgia that was not forecast operationally.

Six hours later (0600 UTC 26 January) (not shown) this cyclonic circulation was evident over eastern North Carolina as the low that formed on the coastal front off Georgia moved northward along the front. By 1200 UTC 26 January (Fig. 3) the subsynoptic cyclone was now a 1006 mb low analyzed near Washington, D.C. with the coastal front displaced further offshore by the westerly winds behind the low as it moved north along the coast. The main low pressure system which was originally over Texas had progressed to southern Georgia with a pronounced trough of low pressure stretching along the coast from Florida to New England. Behind the coastal front was a sharp gradient of moisture at the surface. Also strong cold advection was developing over the midwest behind the main trough. By 1800 UTC 26 January the low pressure center progressed northeast, with the front moving further offshore.

4. Results

a. General structure

Although the models are integrated for 30 h, the 24 h forecasts are selected for presentation in sections 4a and 4b because the 30 h analyses (valid at 1800 UTC 26 January) are not as complete. The 30 h forecasts will be used in section 4c for the comparison with aircraft data. Also because the front and cyclone are of the most interest here, the results presented are only over a portion of the model domain, from 70°–90°W and 30°–45°N.

After 24 h of integration all three models, M10, MB16 and EE16, developed the coastal front system along the East Coast with the surface low pressure system located near Delaware and New Jersey (Fig. 4). Thus the system develops regardless of the type of PBL parameterization. With the initial conditions favorable for this development, namely, a strong land–sea temperature difference and onshore flow with strong upper-level support, the 3-D model forecasts of the larger mesoscale system are not extremely sensitive to model changes in PBL parameterizations. Statistical analysis involving rms errors and S_1 scores of the 24 h SLP field confirm this result. These scores are commonly used to evaluate horizontal gradients, with a value of 30 for SLP representing a "perfect" forecast and a value of
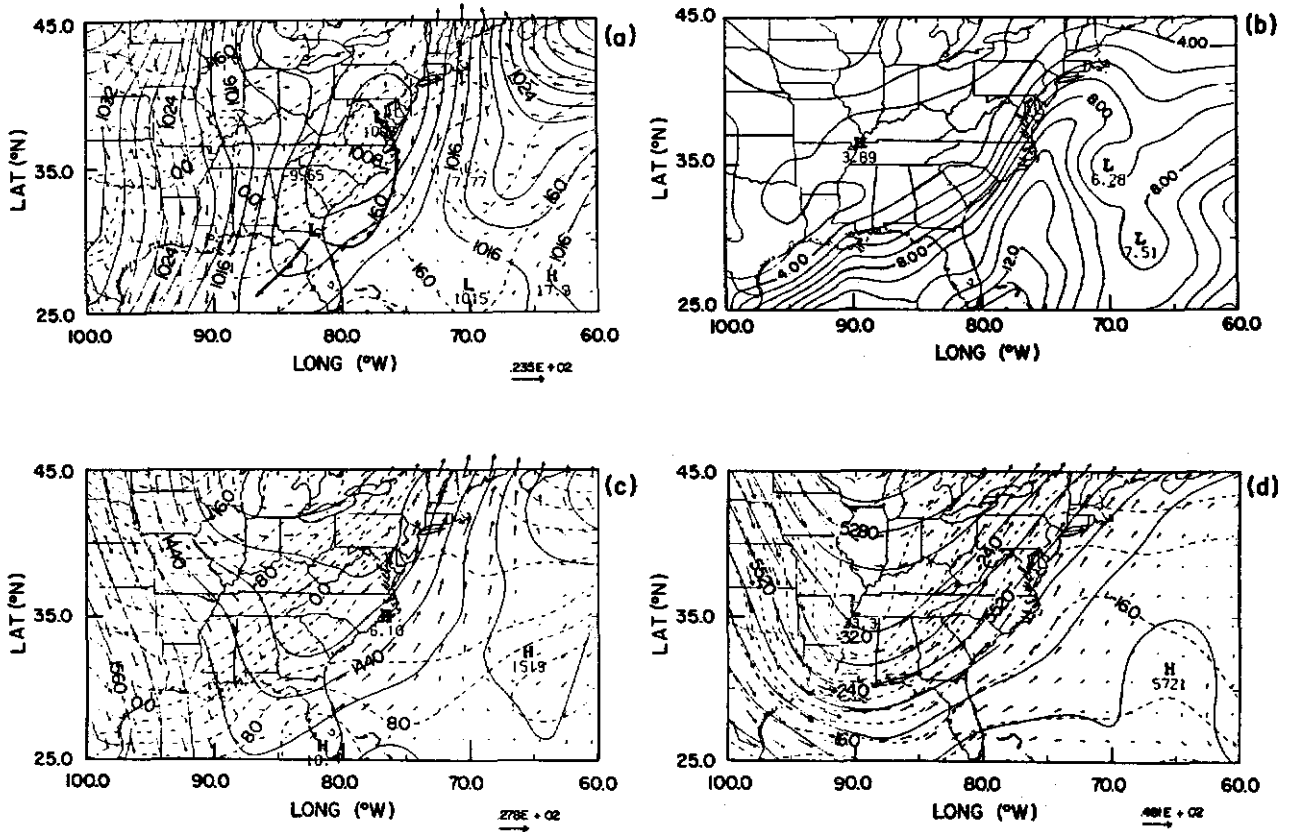
FIG. 3. NMC/RAFS analyses at 1200 UTC 26 January 1986 as in Fig. 1.

80 representing a relatively useless forecast (Anthes 1983; Fawcett 1977). The S_1 score of 54 for model EE16 as compared to scores of 55 and 60 for models MB16 and M10, respectively, indicates EE16 provides a slightly better forecast of the overall SLP gradient. The S_1 scores computed over the whole model domain for all three models are approximately 40 and are less than the smaller domain because the smaller domain is influenced more by the low pressure center where the pressure gradient is large. The rms errors of SLP range from 3.3 mb for M10 to 4.0 mb for EE16.

The simpler model M10 agrees better with the most sophisticated model EE16 and with observations in the position and strength of the front than the relatively more complex model MB16. The parameterization used in MB16 has the same bulk formulation at the lowest level as M10, but the depth over which this bulk formulation is assumed valid differs. As seen in Table 1, the lowest model level for MB16 is approximately $\sigma = 0.9975$ compared to $\sigma = 0.95$ for M10. For M10 this depth is assumed as the depth of the PBL, i.e., the lowest model layer contains the entire PBL (approximately 1 km). For the region and time period considered in this study, this assumption proves to be adequate, partially explaining the good forecasts by M10. The formulation for MB16, however, while using the

bulk formulation at its lowest level, also contains a mixing-length formulation for the remaining six levels up to approximately $\sigma = 0.86$ considered to be representative of the PBL. The mixing-length formulation is that of Blackadar (1962) in which vertical mixing is a function of mixing length and shear. Separate stability modules, such as those proposed by Zhang and Anthes (1982) for stable and unstable atmospheric conditions, are not included. This parameterization is chosen because of its relative simplicity. The major drawback of this scheme as it is included here, however, is that it is not a function of stability. Spuriously large K_m and hence large vertical mixing particularly at the top of the PBL can be generated based on this scheme, as emphasized by Holt and Raman (1988) for 1-D model simulations. This mixing reduces the low-level baroclinicity by transporting heat away from the surface and weakening the horizontal definition of the frontal zone. This is the reason the surface frontal zone forecast by MB16 at 24 h (Fig. 4c) is much broader and more difficult to determine.

Model EE16 shows the largest intensification of the surface low near southern New Jersey (Fig. 4d), though only by 2 mb—1001 mb versus 1003 mb for M10 and MB16. The differences in the physical parameterization of the PBL, particularly the surface boundary layer,
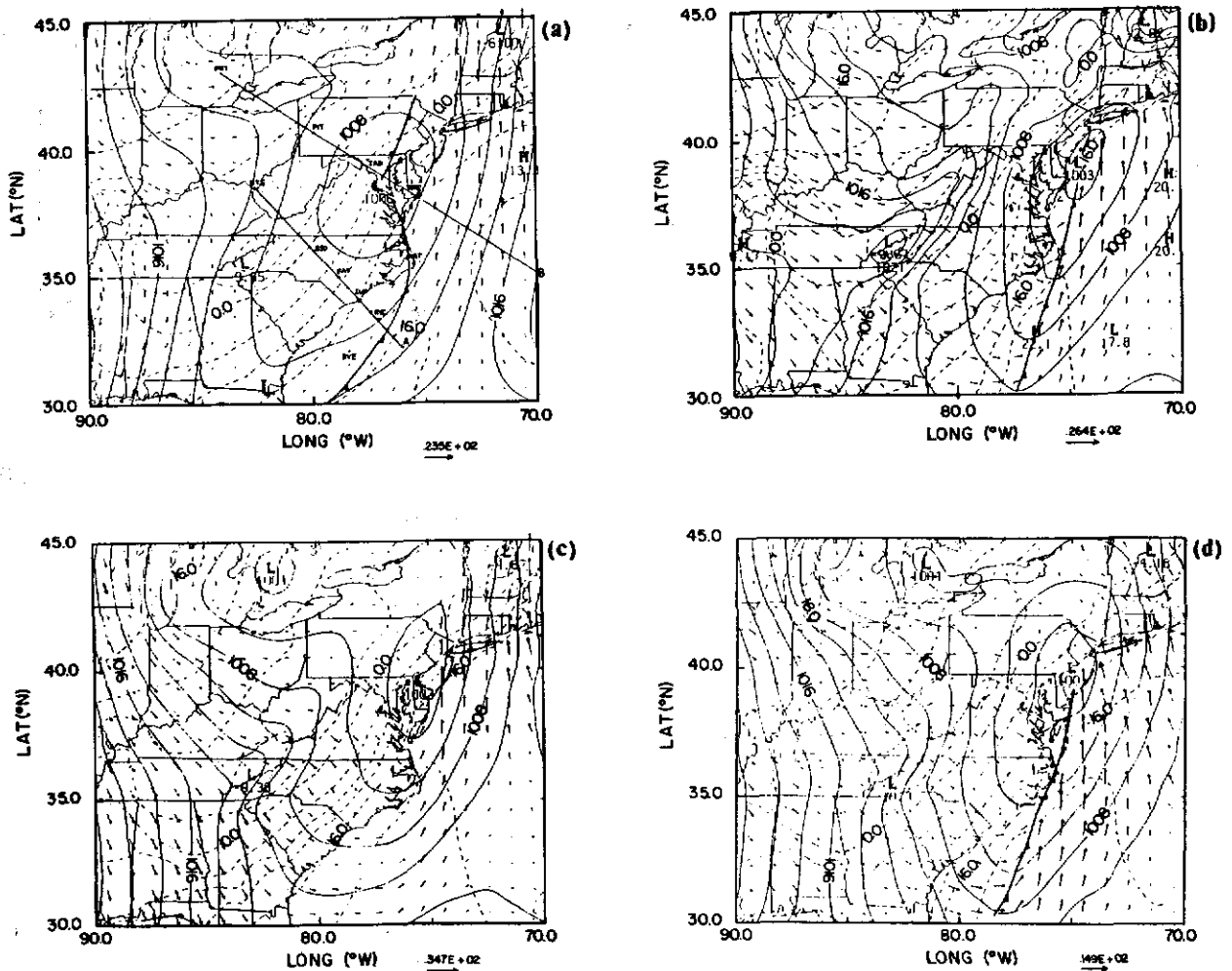
FIG. 4. Sea level pressure (solid lines, mb), surface winds (vectors, m s^{-1}) and temperature (dashed lines, C) valid at 1200 UTC 26 January 1986 for (a) NMC/RAFS observations, (b) model M10, (c) model MB16 and (d) model EE16. Frontal position is also indicated. Cross sections and soundings are given in panel (a).

should affect the intensification. With the low generally forming and moving along the coastal regions, the differences in friction velocity u^* over land and over water as well as differences in latent and sensible heat fluxes should be important. The maximum frictional drag at 12, 18 and 24 h for models M10 and MB16 (0.90 N m^{-2}) and EE16 (0.46 N m^{-2}) is larger just offshore in association with the development of the coastal low near Delaware and New Jersey than onshore. At 24 h for model EE16, maximum momentum flux extends from just offshore of North Carolina to offshore of New Jersey. The momentum flux near the coast over land was significantly smaller (0.1 N m^{-2}) than fluxes over the ocean for all models. Thus, reduced frictional drag along the coast could be a contributing factor in the greater intensification of the surface low.

Chang et al. (1989) and Nuss and Anthes (1987) emphasized the importance of low-level baroclinic in-

stability and its relationship to the distribution of surface sensible and latent heat fluxes in the intensification of surface cyclones. Heat flux distribution at 12 h (0000 UTC 26 January) during the developmental stage of the surface low supports the hypothesis that heat fluxes play an important role in the intensification of the low. During this developmental stage, all models show weak sensible and latent heat fluxes over the ocean north of North Carolina to New Jersey, indicating little low-level modification to the baroclinic zone established across the warmer ocean and colder land. Over land, however, a surface energy budget is used in model EE16 to calculate surface temperature and sensible heat fluxes, while models M10 and MB16 have no sensible heat flux over land. The inclusion of these fluxes reduces the low-level static stability near the coastal regions contributing to slightly greater intensification of the surface low.

To further examine the importance of surface fluxes in the development of the coastal front system, an additional 24 h simulation that had no surface sensible or latent heat fluxes was performed for model MB16. Model simulations valid at 1200 UTC 26 January shown in Fig. 5 emphasize the importance of flux contributions to the development of the coastal front system. Compared to the observations and model simulations with heat fluxes (Figs. 3 and 4), the no-flux case does not develop a coastal front or coastal low. The absence of the strong baroclinic zone observed over North and South Carolina is also obvious in the no-flux case. The trough of low pressure observed along the East Coast evident up to 850 mb at 1200 UTC 26 January also is lacking. At 500 mb without fluxes, model simulations fail to show a deepening of the trough. The largest amounts of precipitation in the no-flux simulation (Fig. 5d) are generally offshore near 37.5°N, 65°W with lesser amounts forecast in the Ohio Valley associated with the frontal system. This contrasts with both the observed precipitation fields and model simulations with surface fluxes shown in Fig. 6. The observed field (Fig. 6a) was derived from three data sources. In the inner GALE region, precipitation totals were obtained from the PAM network while other precipitation amounts over land were from NMC observed

24 h totals. Over the ocean, precipitation amounts were from satellite estimates (Martin et al. 1988). Maximum precipitation occurs along the coast in association with the frontal system. Without the development of the coastal front system, model simulations without fluxes are not able to correctly forecast the observed maximum precipitation along the coast from HAT north New York City.

In addition, development and subsequent intensification of the coastal front system for 25–26 January does not occur without surface fluxes of latent and sensible heat. The rms error for SLP (6.4 mb) and S_1 score (84) for the no-flux case are much larger than the values for simulations with fluxes, indicating little forecast skill in predicting the development and intensification of this cyclone. This importance of surface fluxes on cyclogenesis agrees with the results from other studies (Chen and Dell'Osso 1987; Davis and Emmanuel 1988). Others (Danard and Ellenton 1980; Nuss and Anthes 1987; Chang et al. 1989), however, have shown surface fluxes to actually reduce intensification and deepening of the cyclone. The phase and magnitude of the fluxes relative to the low-level baroclinic zone is an important factor (Nuss and Anthes 1987; Kuo and Reed 1988). Regions of positive diabatic heating anomalies (positive surface sensible heat flux or latent
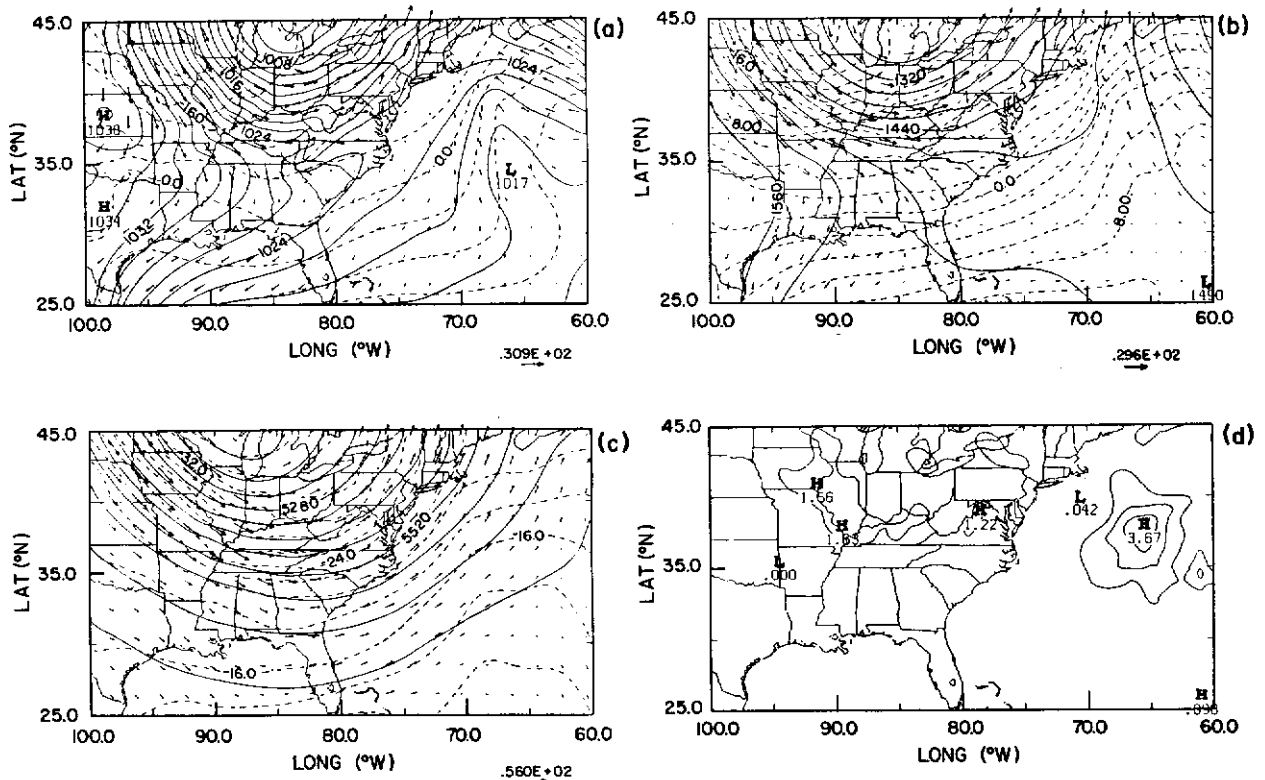

FIG. 5. Model forecasts of MB16 valid at 1200 UTC 26 January 1986 for the no-flux case: (a) sea level pressure (solid lines, mb), surface winds (vectors, m s^{-1}) and temperature (dashed lines, C); (b) 850 mb winds (vectors, m s^{-1}), temperature (dashed lines, C) and geopotential (solid lines, m); (c) 500 mb winds, temperature and geopotential and (d) accumulated total precipitation (cm).
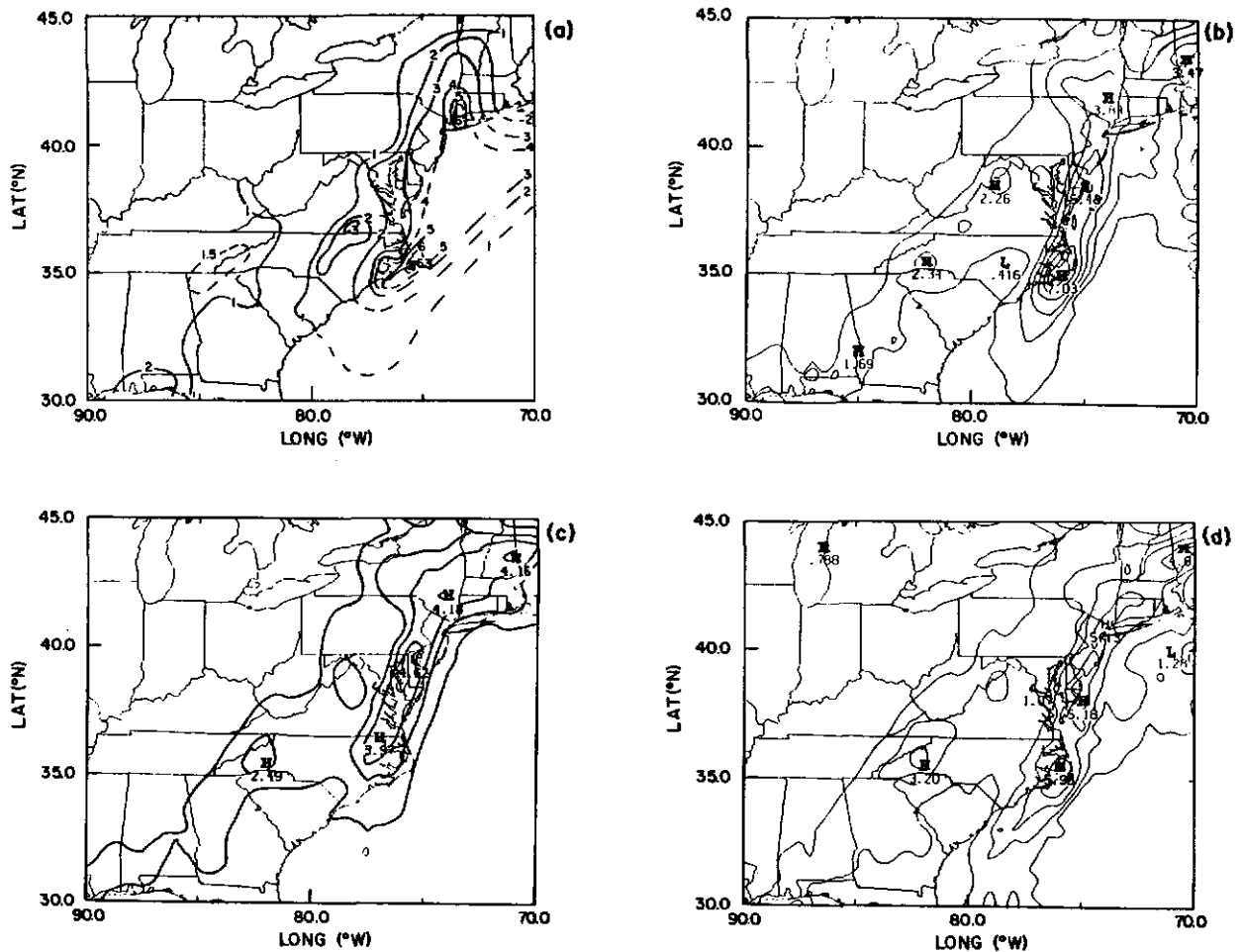
FIG. 6. Accumulated 24 h total precipitation (cm) valid at 1200 UTC 26 January 1986 for (a) observations,
(b) model M10, (c) model MB16 and (d) model EE16.

heat release) contribute to cyclonic development. Typically these regions of heating do not occur ahead of the developing system (Petterssen et al. 1962), and thus the system is somewhat damped; however, heat fluxes for 26 January (Figs. 7 and 8) calculated by the bulk aerodynamic method (Akkarappuram 1988; Friehe and Schmitt 1976) indicate regions of relatively large surface heat flux, particularly latent heat, ahead of the developing frontal system. Conversely, sensible heat flux depends strongly on the location of the front, and thus the magnitude is smaller ahead of the system. This heat flux distribution indicates the possible importance of the low-level latent heat flux in the vicinity of the Gulf Stream in enhancing cyclone development for this case.

The lack of development of the coastal system for simulations without fluxes (Fig. 5) gives credence to the assumption of no sensible or latent heat flux over land used in models M10 and MB16 in which the cyclone did form. The fact that the three models develop

the subsynoptic cyclone at 24 h (1200 UTC 26 January) (Fig. 4) indicates that surface sensible and latent heat flux over land are of limited importance. In contrast, the lack of such cyclonic development seen in Fig. 5 emphasizes the importance of these fluxes over the ocean.

b. Vertical structure

Two regions are considered here to help assess the relative importance of a more complex PBL parameterization versus increased vertical model resolution. One is the area in which topographical forcing is important, namely, areas in the vicinity of the Appalachian Mountains. The second is the area in which land–air–sea interactions are important, namely, the coastal and Gulf Stream regions.

Given in Fig. 9 are the hand-analyzed cross section obtained from the high vertical resolution (10 mb) CLASS observations with a horizontal resolution of
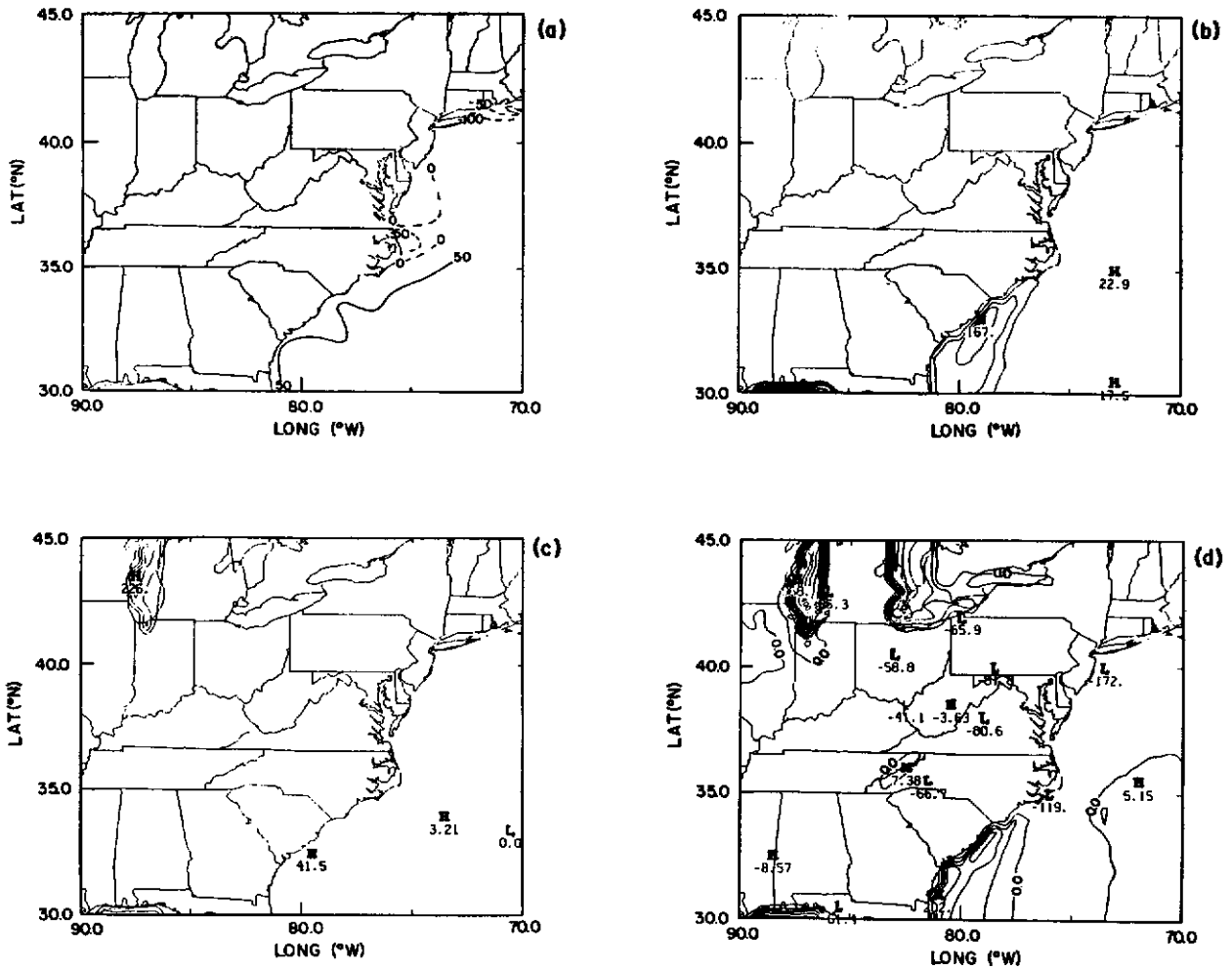
FIG. 7. Same as Fig. 6 but for sensible heat flux (W m^{-2}). Values for model MB16 (c) were all less than 50 W m^{-2} over the ocean.

approximately 1°–1.5°, the computer generated cross section of 2.5° horizontal resolution NMC/RAFS analysis, and the three model simulations. The NMC analysis with less horizontal resolution than the CLASS observations lacks a sharp temperature gradient across the front. From the comparison of the cross section of potential temperature across the frontal zone, the increase in vertical model resolution of MB16 does not noticeably improve model forecasts of the temperature structure of M10 behind the front near the mountains. The same is true for the cross section circulation given in Fig. 10. The three model simulations given in Fig. 10 show strong subsidence behind the frontal position which slopes back over the Appalachians as generally observed (Anthes et al. 1983; Atkinson 1981; Browning et al. 1973, 1974). Low-level flow behind the front typically seen in observations or modeling studies is restricted here by the presence of the mountains to the west. Thus, the flow parallel to the mountains (i.e., out of the paper), evident only in model EE16 (Fig. 10c),

is a direct result of this circulation behind the front. With MB16 not simulating this feature, it is presumed to be due to the improved PBL parameterization and not the increased vertical model resolution. Numerical values of subsidence are roughly equal for each simulation (40–45 mb h^{-1}) although subsidence is stronger above 700 mb for model EE16 than for M10 or MB16 possibly due to increased turbulent exchange with the overlying free atmosphere.

An example of the effects that a change in PBL parameterization can have in the vertical is seen in the cross section circulation through the main low pressure system (Fig. 11). Consider the flow just east of the mountains near Dulles (IAD) in which all model simulations show weak subsidence behind the front sloping back over the mountains. The interesting difference in model simulations is the typically observed zone of rising motion that originates from near the surface and slopes back and overrides the subsiding cold air, which is best modeled by EE16. Model MB16 hints at a region
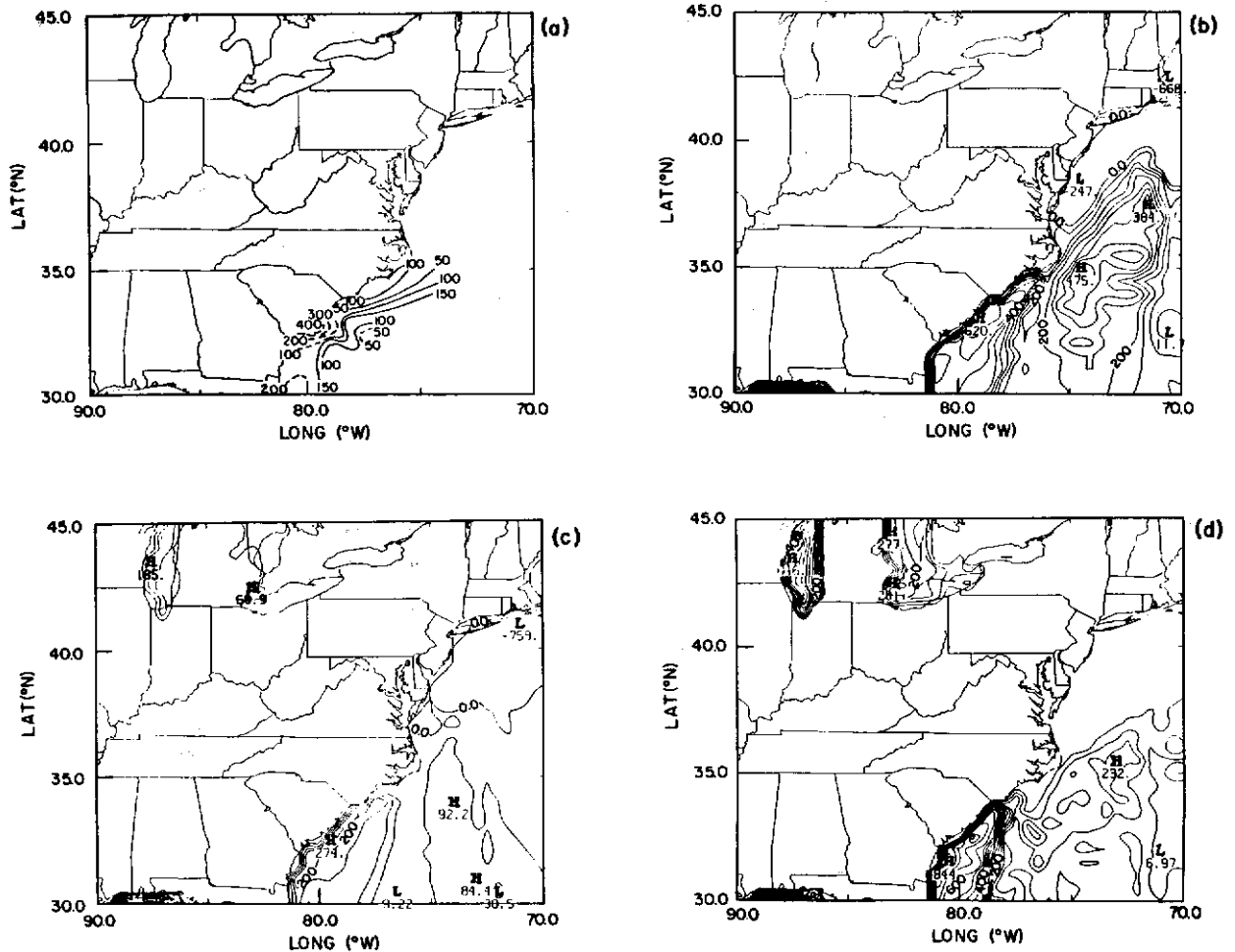
FIG. 8. Same as Fig. 6 but for latent heat flux ($W \, m^{-2}$).

of ascending air between Pittsburgh, Pennsylvania (PIT) and IAD from 700 to 500 mb, but the fact that no ascending motion is forecast by MB16 in the PBL near IAD suggests that the improved PBL parameterization of EE16 is important. Model M10 shows a narrow region of ascending motion in the PBL near IAD from 950 mb to 800 mb but this region combines with the region of ascending motion associated with the frontal boundary to the east near Wallops Island, Virginia (WAL) instead of sloping back to the west over the colder air as expected. Only model EE16 forecasts two distinct zones of ascending motion in the PBL. Weak descending motion is forecast between the two zones, which are separated horizontally by only approximately 75–100 km. In the vicinity of the mountains, increased vertical model resolution, though important, is not as vital as a proper PBL parameterization in improving forecasts of low-level frontal structure and the associated circulation. Important processes such as increased horizontal and vertical turbulence generated from topographical forcing, though capable

of being better resolved with a finer vertical grid, may not be properly simulated because of deficiencies in the PBL parameterization.

A similar conclusion can be drawn upon consideration of the frontal structure and circulation in the vicinity of the coastal and Gulf Stream regions. Differences in the horizontal and vertical flow fields in the region of strong upward motion near the Gulf Stream at 24 h associated with the frontal system are evident in the vertical cross section of circulation (Fig. 10). Of the three models, EE16 shows the most narrow zone of rising motion over the surface position of the front similar to that typically observed and modeled, for instance, by Anthes et al. (1983) or Keyser and Anthes (1982). Maximum updrafts in the frontal region as forecast by EE16 are similar to other coastal front studies (Bosart 1981)—approximately 50–60 mb h^{-1} at 750–850 mb compared to 40–50 mb h^{-1} at 800–850 mb for M10 and 40–50 mb h^{-1} at 600–700 mb for MB16. Comparison of the horizontal structure of the updraft region, however, shows a much more in-
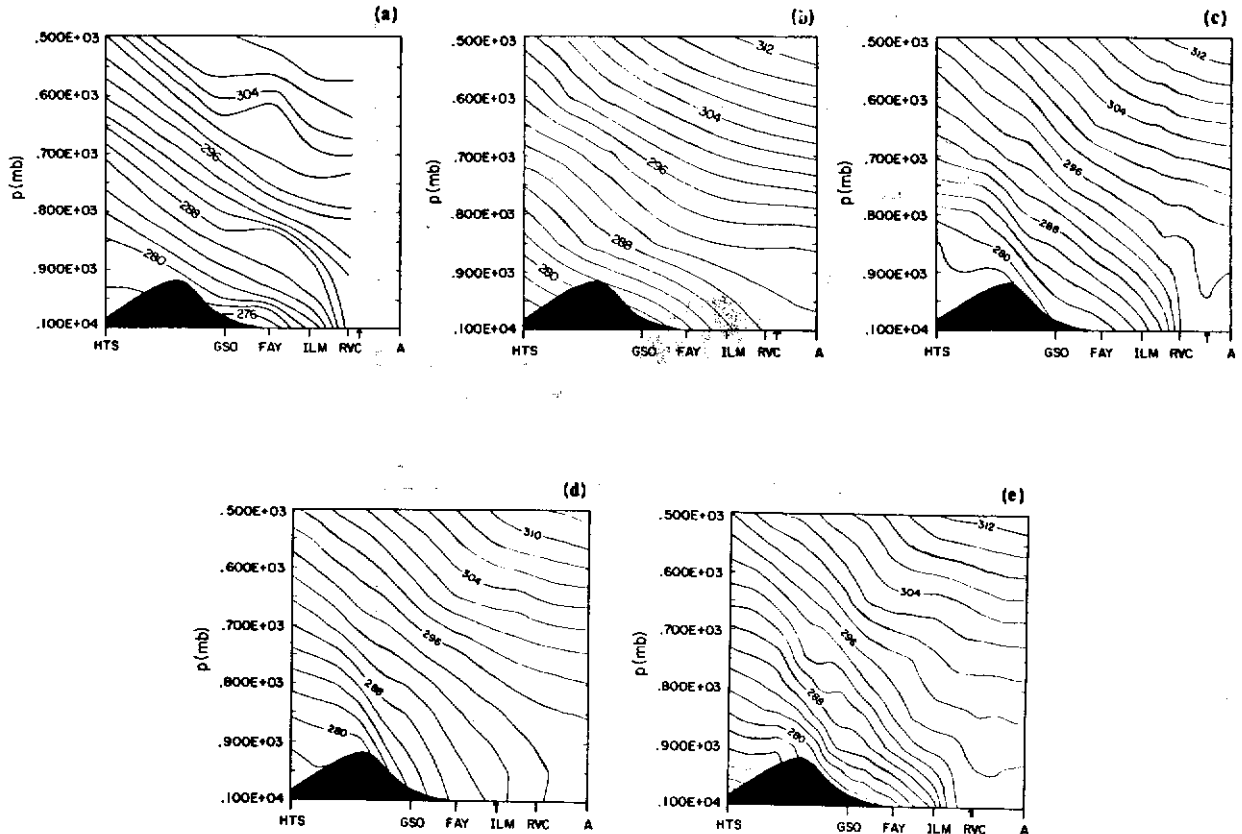
FIG. 9. Vertical cross section of potential temperature Θ (K) from Hunington, West Virginia (HTS) to point A shown in Fig. 4a valid at 1200 UTC 26 January for (a) CLASS observations, (b) 2.5° NMC/RAFS analysis, (c) model M10, (d) model MB16 and (e) model EE16. The vertical coordinate is pressure (mb). The arrow along the abscissa indicates the position of the surface front.

tense region of ascent in EE16 compared to much broader and less well defined regions of ascent in M10 and MB16. Model M10 particularly, with no effects of PBL mixing above roughly 950 mb, indicates a broad updraft region of almost 100 km, compared to only 60 km for EE16.

Also evident in the wind field in the vicinity of the offshore front is the presence of a low-level jet as forecast by model EE16 (Figs. 12 and 13). The presence of a warm low-level southerly jet ahead of the cold front has been documented observationally (Ogura and Portis 1982; Shapiro 1983). Although no observations are available over the ocean, the poorer resolution NMC/RAFS analysis (Figs. 12b, 13b) still hints at possible high winds in the lower troposphere offshore. The numerical study of Keyser and Anthes (1982) showed the importance of a proper parameterization of PBL fluxes, particularly momentum, in the development of the low-level jet. Keyser (1986) emphasized that the depletion of along-front momentum flux in the PBL by friction could cause subgeostrophic winds near the surface. Also above the surface layer in the PBL, maximum ageostrophic flow toward the front would be expected resulting in a low-level wind max-

ima. In model simulations of M10 and MB16, no low-level jet is forecast. Model M10 has the disadvantage of only one level in the PBL and thus could not properly resolve the momentum and frictional effects. Model MB16 has sufficient resolution but lacked an adequate PBL parameterization. Thus, without proper parameterization of turbulent fluxes in the PBL or accurate determination of surface frictional drag, development of the low-level prefrontal jet is not possible.

The low-level jet behind the front forecast only by model EE16 (Figs. 12e, 13e) is also seen in the CLASS observations, but the analysis shows it to be weaker and limited in horizontal extent due to the poorer resolution of the CLASS network. The NMC/RAFS analysis shows no postfrontal low-level jet. The sounding at IAD suggests a possible low-level jet between IAD and Pittsburgh (PIT); however, the magnitude and horizontal extent of this jet cannot be substantiated.

The inadequate handling of atmospheric stability in the PBL parameterization for MB16 is also evident in the vertical structure of the atmosphere, particularly the intensity and definition of the sloping baroclinic zone. The comparison of vertical sounding profiles at
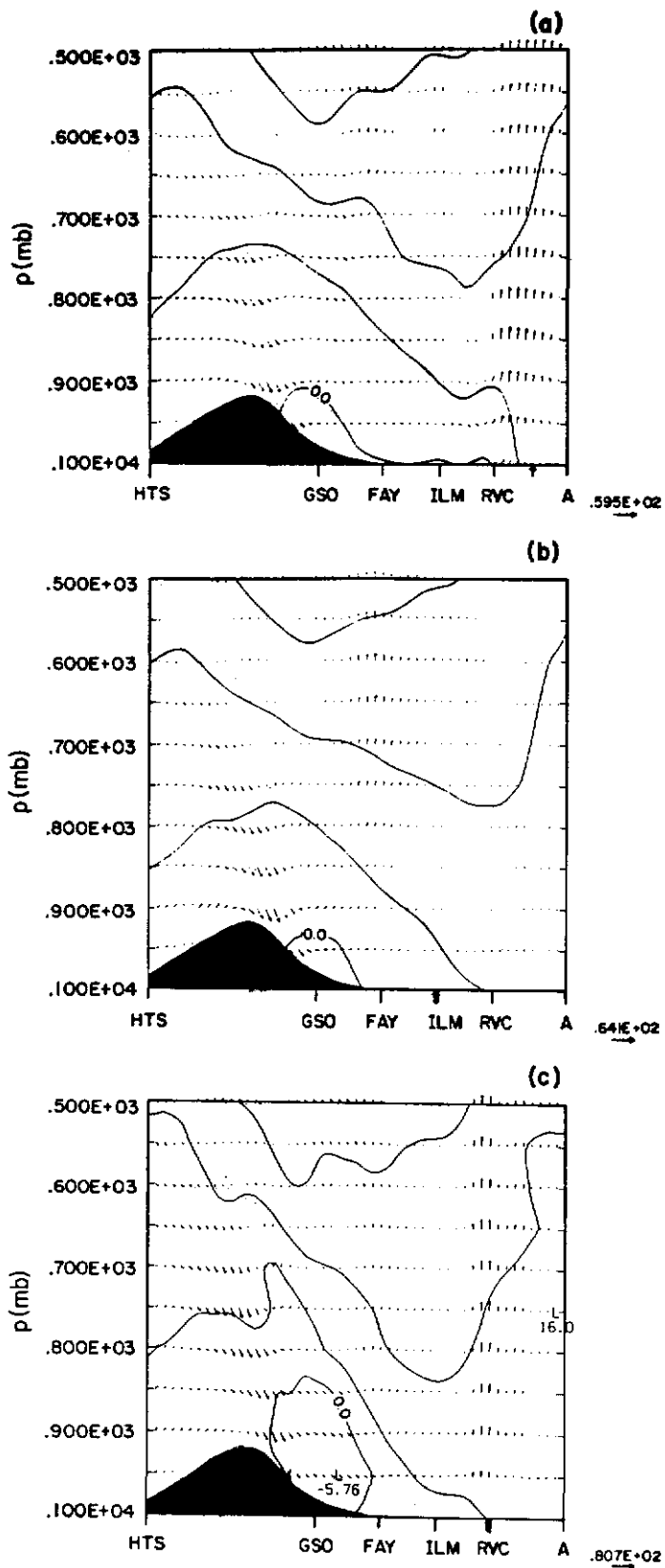
FIG. 10. Vertical cross section of circulation valid at 1200 UTC 26 January for models (a) M10, (b) MB16 and (c) EE16. Winds normal to the cross section are contoured positive into the paper. Tangential and normal winds are represented by vectors with the maximum vector given in the lower right corner. Normal and tangential winds are m s^{-1} while vertical winds are mb h^{-1}.
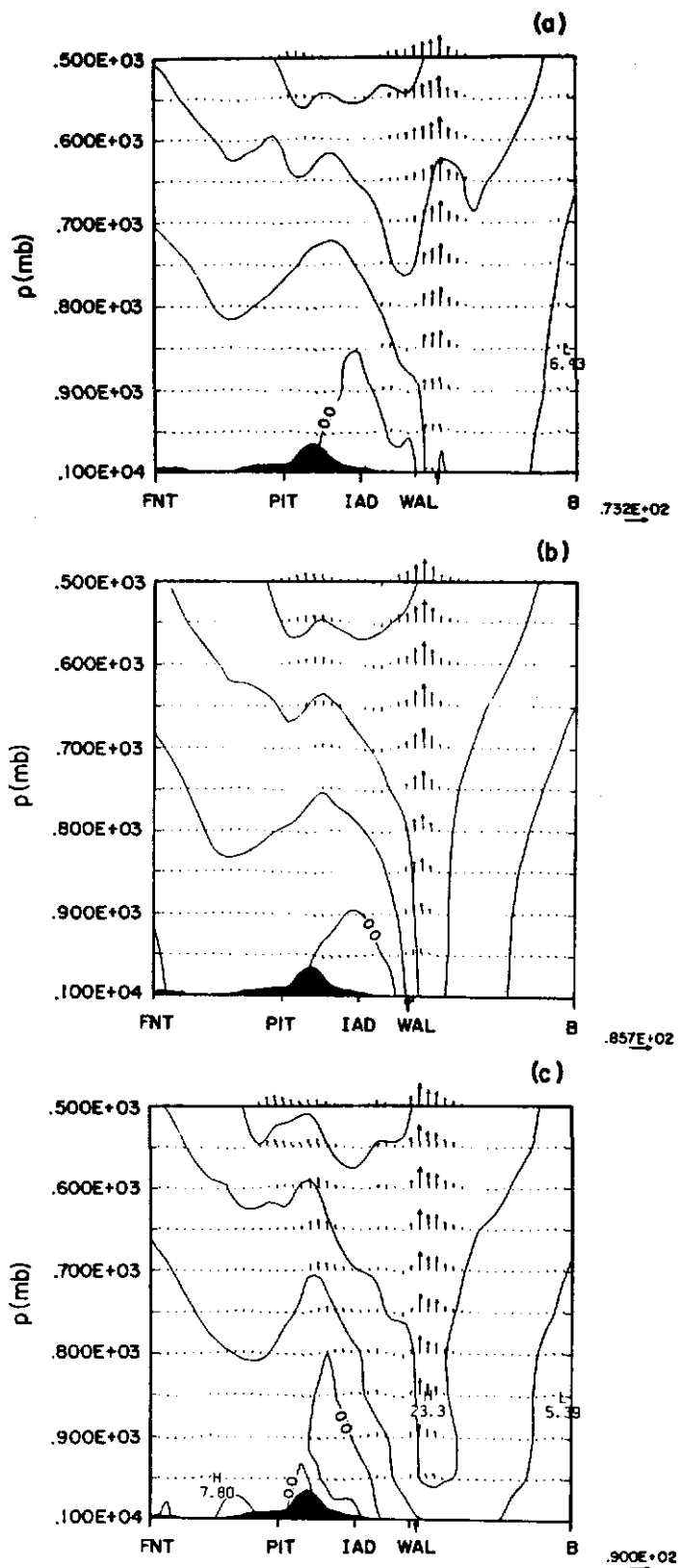
FIG. 11. Vertical cross section of circulation from Flint,
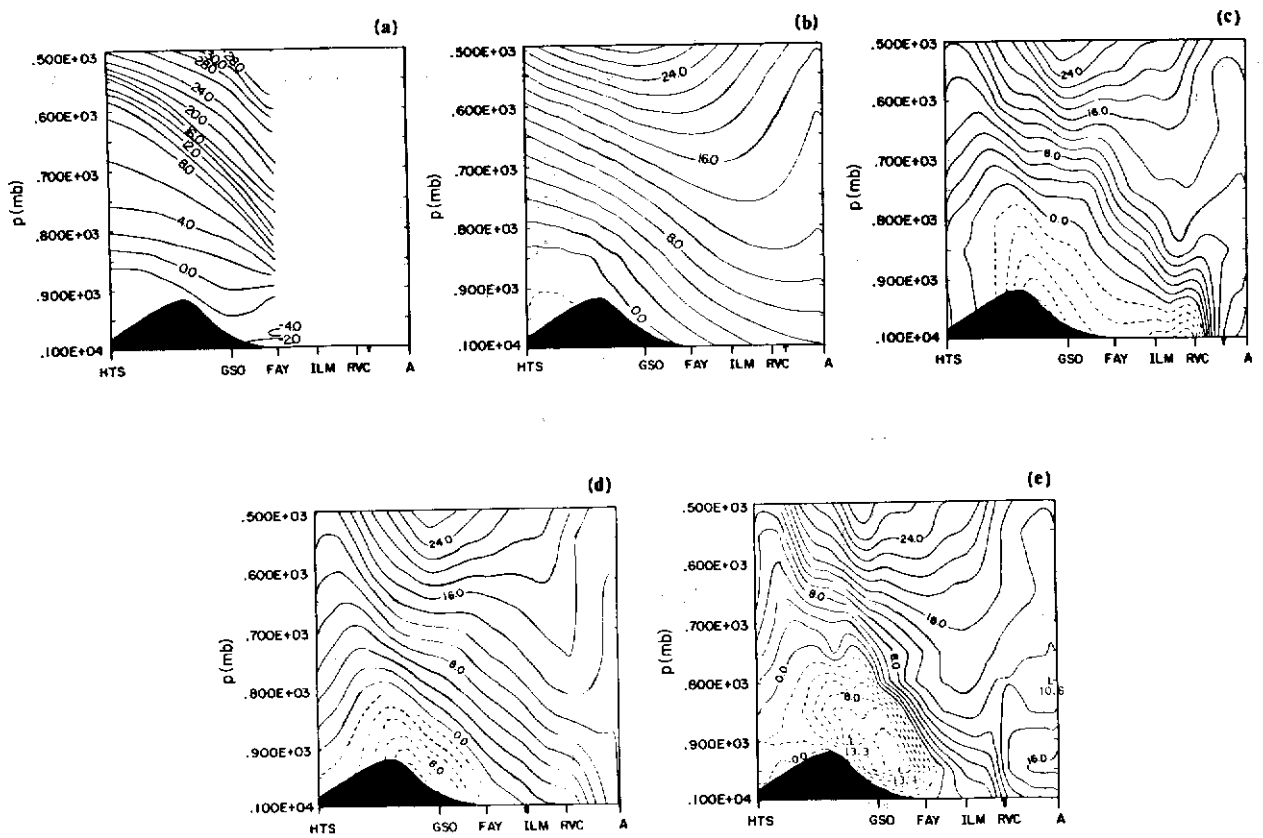Michigan (FNT) to B similar to Fig. 10.

FIG. 12. Vertical cross section of north–south wind component V (m s^{-1}) from HTS to point A shown in Fig. 4a valid at 1200 UTC 26 January for (a) CLASS observations, (b) 2.5 ° NMC/RAFS analysis, (c) model M10, (d) model MB16 and (e) model EE16.
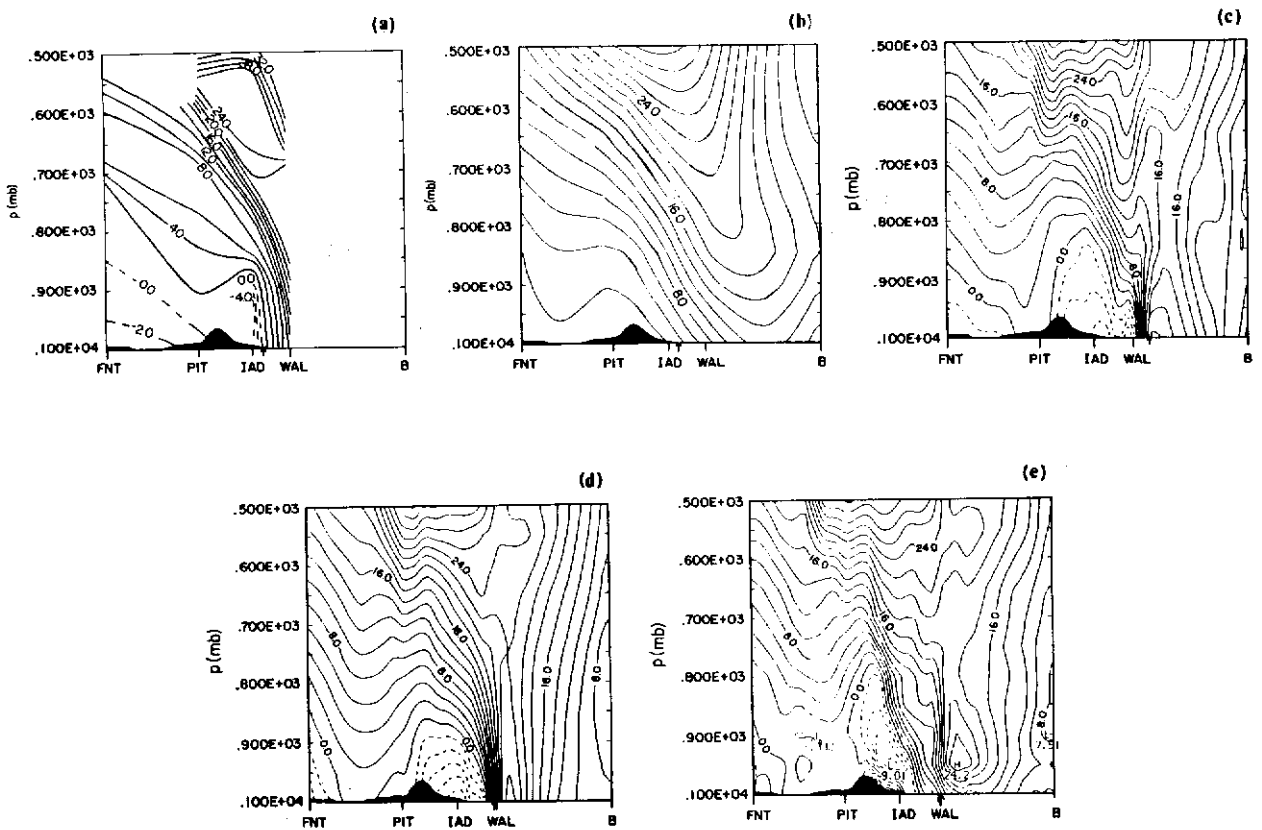

FIG. 13. Same as Fig. 12 but for north–south wind component V (m s^{-1}) from FNT to point B.

Cape Hatteras, North Carolina (HAT), the Research Vessell *Cape Hatteras* (RVC) and the Research Vessel *Endeavor* (RVE) emphasizes this result. Of the three, the station in which the stability deficiency of the PBL parameterization of model MB16 should be most evident would be HAT. This is because it is located over land with a stronger early morning 1200 UTC low-level stable layer evident compared to RVC and RVE located over the warmer ocean (Figs. 14, 15 and 16). A transitional period, such as early morning, characterized by changing stability conditions, would be most difficult for MB16 to model accurately. Thus, the better-mixed boundary layer predicted by MB16 (Fig. 14c) as compared to EE16 is to be expected. The low-level stable layer correctly forecast by EE16 is not evident for MB16 due to upward vertical mixing resulting in

a smoother temperature profile. The wind profiles at HAT forecast by MB16 also show a better-mixed profile than observed. The conclusion is that better vertical resolution in the lower troposphere alone is insufficient to model the PBL properly.

The marine boundary layer in the cold air regions behind the front typically shows a better-mixed and deeper cloud-topped PBL than the regions ahead of the front in the warm air (Bond and Fleagle 1988). A good example of frontal passage and changes in boundary layer structure and processes is evident in observations and model simulations at the Research Vessel *Endeavor* (RVE). At 24 h the observed surface front had passed RVE and was located approximately 75 km to the east (Fig. 4a). Model simulations for M10 and EE16 also position the front to the east of
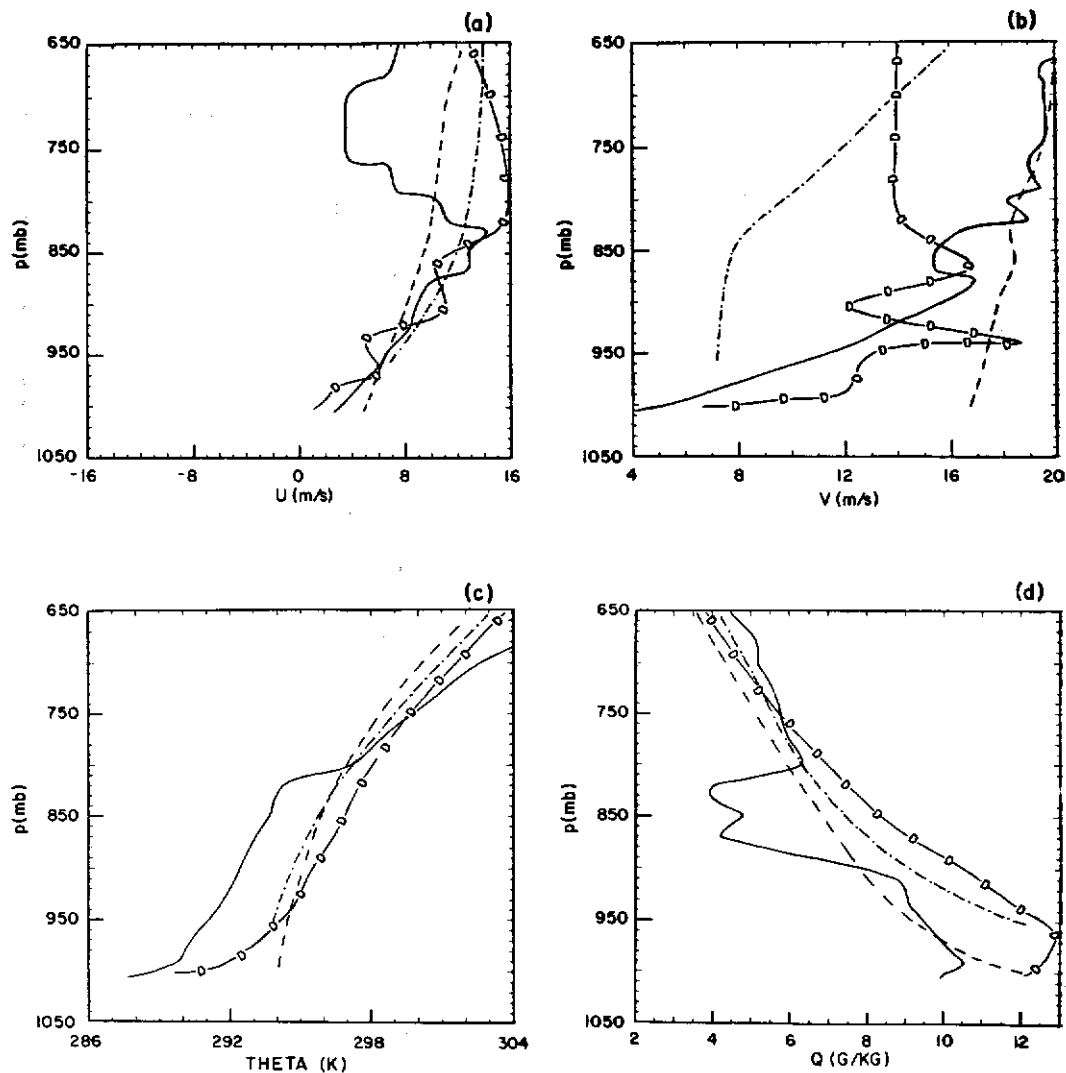

FIG. 14. Vertical sounding profiles at Cape Hatteras, North Carolina (HAT) valid at 1200 UTC January for (a) east–west wind U (m s^{-1}); (b) north–south wind V (m s^{-1}), (c) potential temperature Θ (K) and (d) specific humidity Q (g kg^{-1}). Observations are given by the solid line, model M10 dot-dashed line, model MB16 dashed line and model EE 16 D-line.
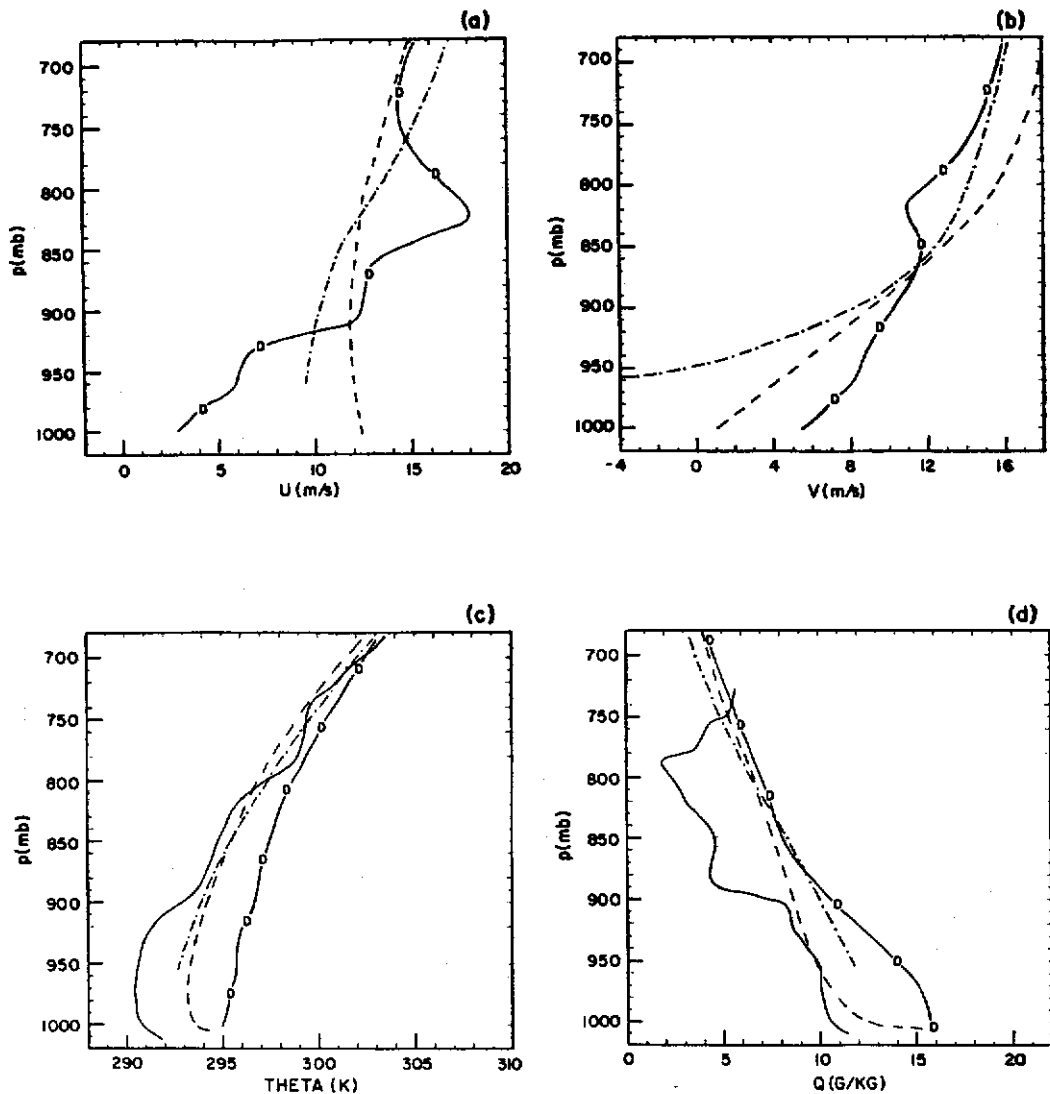
FIG. 15. Vertical sounding profile at the Research Vessel *Cape Hatteras* (RVC) valid at 1200 UTC 26 January similar to Fig. 14.

RVE, but MB16 still had the surface front onshore with RVE in warmer southwesterly flow. As expected, the 24 h observed vertical sounding profile of potential temperature at RVE (Fig. 16c) showed a well-mixed profile up to 930–950 mb even at 1200 UTC (0700 LST). Model M10 simulations, with the surface front forecast to the east, would be expected to show a similar well-mixed temperature structure as observed and as forecast by EE16; however, M10 shows a strong stable layer from 950 mb up through the atmosphere with a smooth linear profile due to limited vertical model resolution. Interpolation between widely spaced data points in the vertical for model M10 severely limits the resolution of small-scale features. Because of the restrictions placed on the PBL parameterization of M10, the lowest data point in the vertical profiles rep-

resents the entire PBL. As seen in the vertical Θ profile at RVE (Fig. 16c), often the bulk parameterization is quite representative of the entire PBL; however, while this one value might be representative of the entire PBL, model M10 is unable to resolve boundary layer structure or depth because of poor vertical resolution. Model M10 often provides only a mean curve through the observations with little vertical structure evident in the wind and moisture profiles at RVE.

The evolution of the TKE budget for model EE16 at RVE (Fig. 17) shows behavior consistent with that observed for typical marine boundary layers as given by Holt and Raman (1989), Chou et al. (1986) and Brost et al. (1982). After 6 h of integration at 1300 LST, the TKE budget at RVE (Fig. 17a) indicates a boundary layer dominated by buoyancy production.
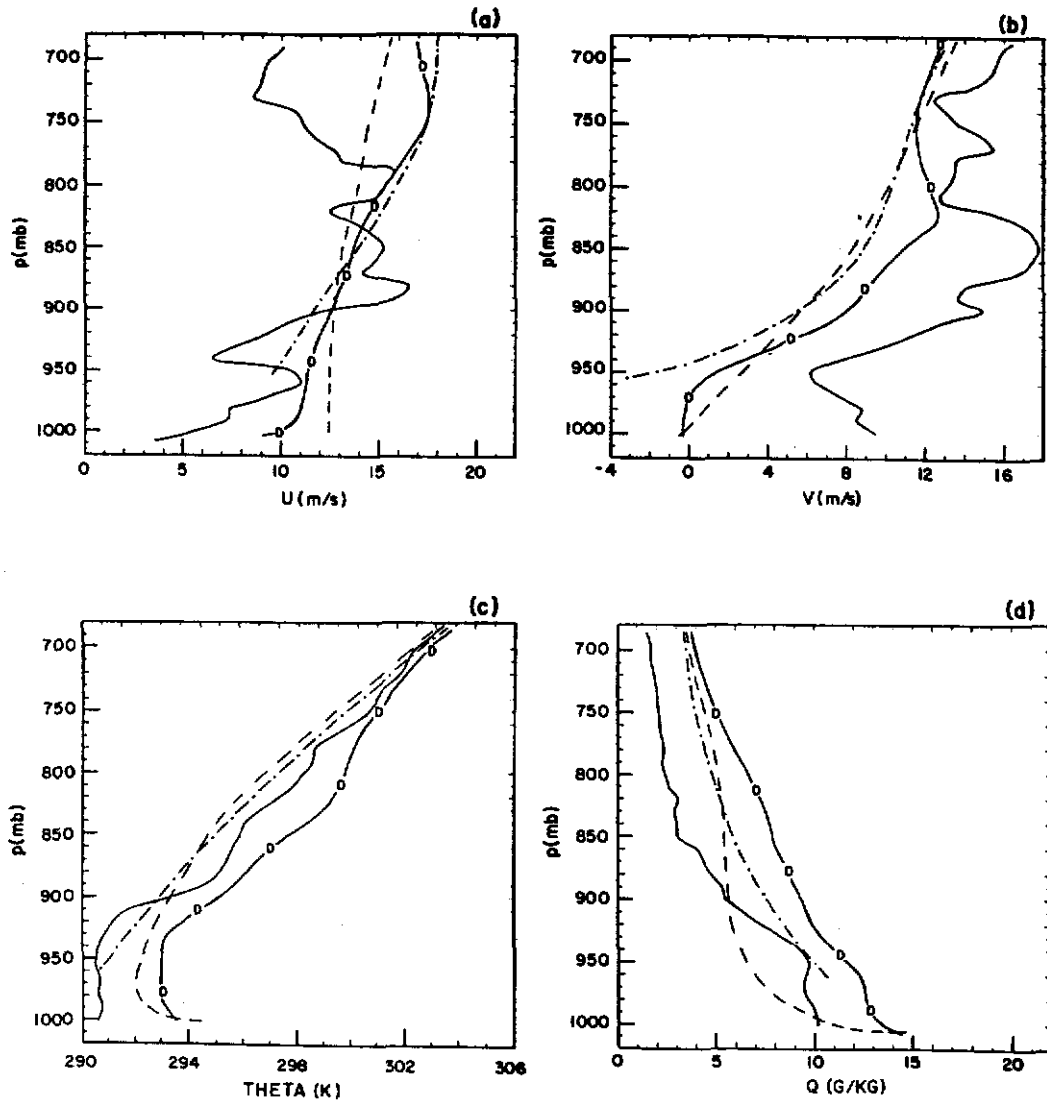
FIG. 16. Vertical sounding profiles at the Research Vessel *Endeavor* (RVE)
valid at 1200 UTC 26 January similar to Fig. 14.

With the winds almost unidirectional and well mixed from the east-southeast (Figs. 18a, b), shear production is less important than buoyancy. It is interesting to note that the sink of TKE in the boundary layer is primarily through turbulent transport out of the PBL and not dissipation. By early evening (12 h: 1900 LST 25 January) buoyancy production is negative, as typically observed, and shear production dominates as model EE16 forecasts a weak prefrontal jet (12 m s^{-1}) at approximately 960 mb. By 18 h (0100 LST 26 January) the stable layer and low-level jet have strengthened considerably, as illustrated by increased negative buoyancy production and positive shear production. Finally, at 24 h, with the front already past RVE to the east, the strong buoyancy production has already broken up the low-level inversion and created a better-

mixed, buoyancy-driven boundary layer typically observed behind the front (Bond and Fleagle 1988). Shear production is an important source of TKE, particularly above approximately 980 mb where a negative buoyancy flux near the top of the boundary layer is observed. Therefore, a noticeable advantage of model EE16 over M10 and MB16 is the incorporation of a more complex physical parameterization. Parameters such as turbulent kinetic energy (E) and energy dissipation (ϵ) used in model EE16 help provide a more physically realistic structure and evolution of the boundary layer.

c. Aircraft data

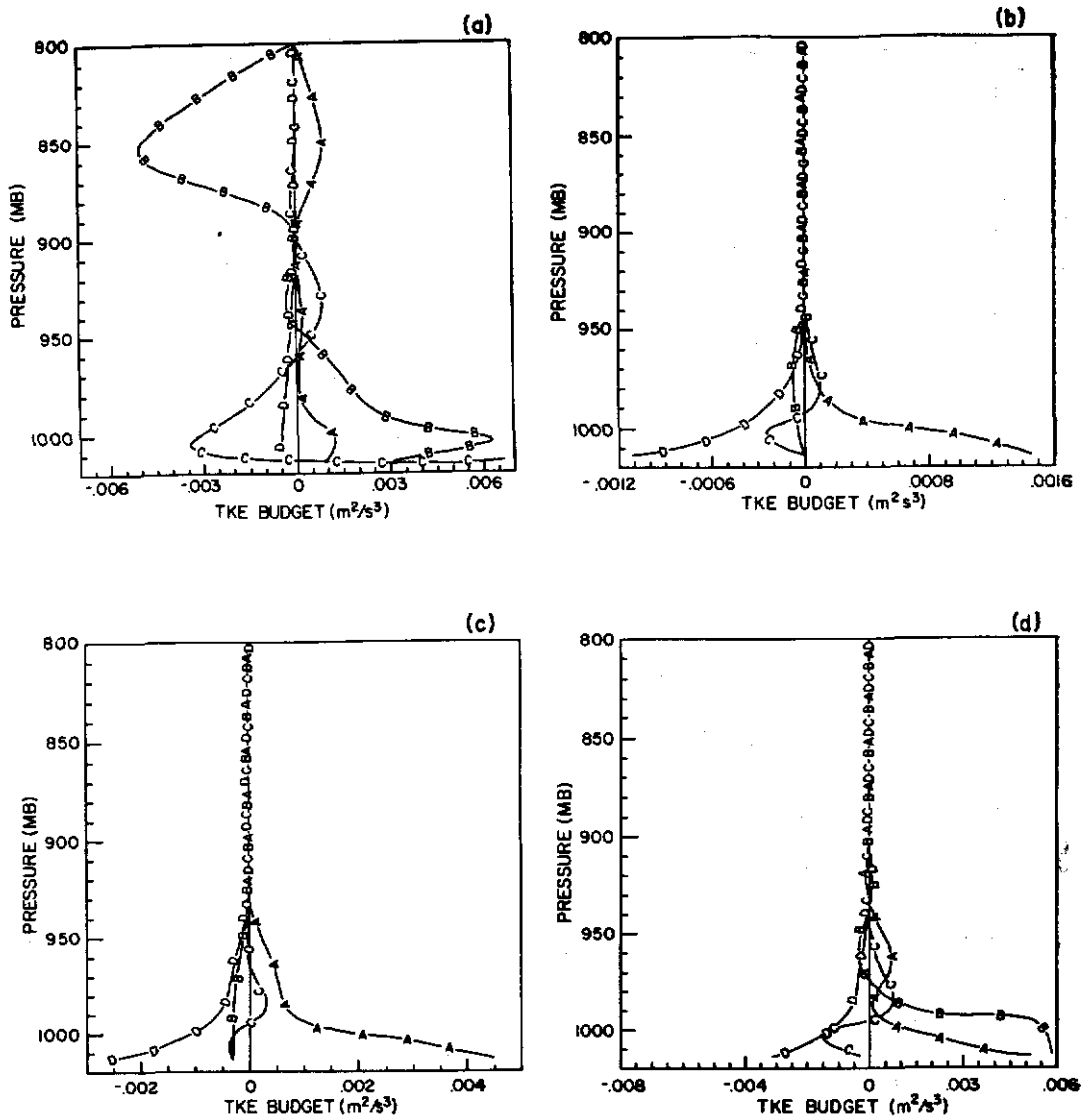Because of the development of the frontal system in the data sparse coastal and oceanic regions, a suitable

FIG. 17. Vertical profiles at RVE for model EE16 of the turbulent kinetic energy (TKE) budget (m² s⁻³) valid for (a) 1800 UTC 25 January (6 h integration), (b) 0000 UTC 26 January (12 h), (c) 0600 UTC 26 January (18 h) and (d) 1200 UTC 26 January (24 h). Profiles are for shear production (A), buoyancy production (B), turbulent transport (C) and dissipation (D).

comparison for the 3-D model results would be mean and turbulent aircraft data obtained over the ocean during this time period. Aircraft data during this time period of GALE IOP-2 were limited to the National Center for Atmospheric Research (NCAR) King Air data near the Research Vessels *Cape Hatteras* (RVC) and *Endeavor* (RVE) at approximately 1700–1800 UTC 26 January, after the frontal passage. Figure 19 shows wind speed and temperature data obtained from the King Air ascent profile at approximately 1700 UTC 26 January near 33.7°N, 77.0°W and model simulations in the vicinity of RVC and RVE. Boundary layer height h, estimated from aircraft data as the height at which turbulence has substantially diminished (ap-

proximately 610 m), is given by the dashed horizontal line. Aircraft ascent profiles at 1700 UTC indicate a well-mixed boundary layer behind the front with no prominent wind speed maxima in the boundary layer. Winds were westerly in the lowest half of the boundary layer backing to southwesterly near $z = h$.

Of the three models considered, model EE16 agrees best with the overall observed vertical structure. From the potential temperature profile, only EE16 predicts the well-mixed boundary layer with a depth comparable to that observed. The magnitude of Θ predicted by model EE16 also shows closer agreement with observations in the boundary layer, overpredicting by 1–2K as opposed to 3–6K for model MB16. Model M10
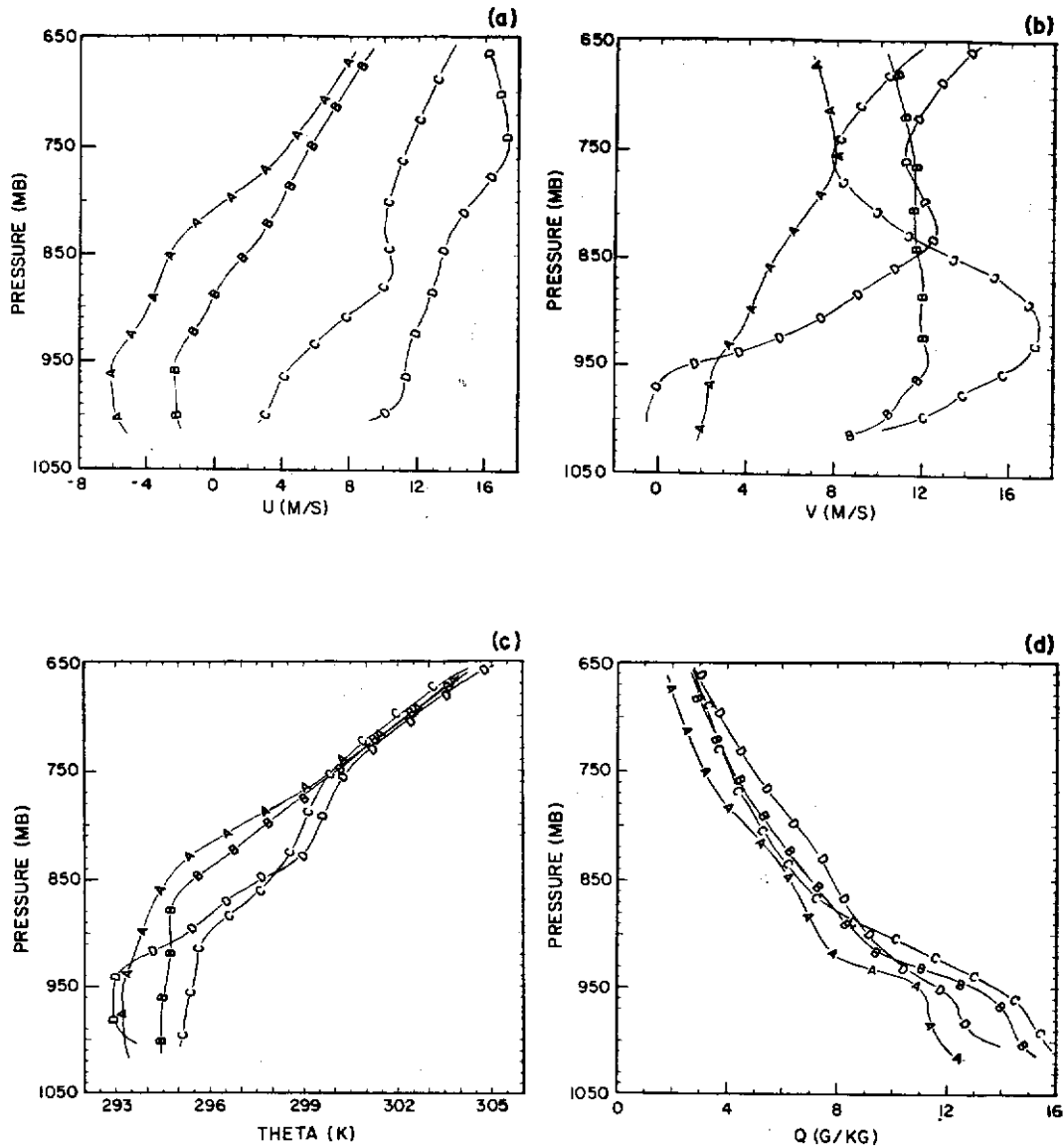
FIG. 18. Vertical profiles at RVE for model EE16 for (a) east–west wind U (m s^{-1}), (b) north–south wind V (m s^{-1}), (c) potential temperature Θ (K) and (d) specific humidity Q (g kg^{-1}). Profiles are valid at 1800 UTC 25 January (6 h integration) —A; 0000 UTC 26 January (12 h) —B; 0600 UTC 26 January (18 h) —C; and 1200 UTC 26 January (24 h) —D.

shows a near-linear profile due to the lack of vertical resolution in the PBL. Wind speed profiles at 1700 UTC indicate observed speeds of approximately 5–6 m s^{-1} throughout the boundary layer compared to 10–14 m s^{-1} for the three simulations.

5. Conclusions

The main conclusions drawn from the comparison of model simulations of the mesoscale structure to observations for the period 1200 UTC 25 January to 1800 UTC 26 January 1986 during GALE IOP 2 are:

1) The TKE boundary layer parameterization scheme shows closest agreement to observations in the regions of the Appalachian Mountains, coastal and Gulf Stream regions in which more complex atmospheric flow is expected. Vertical profiles of turbulent mixing, evident in the structure of eddy viscosity, as well as TKE budgets show good agreement with typical frontal systems. Improvement in forecasts is due primarily to the improved physical representation of the processes that are important in the PBL.

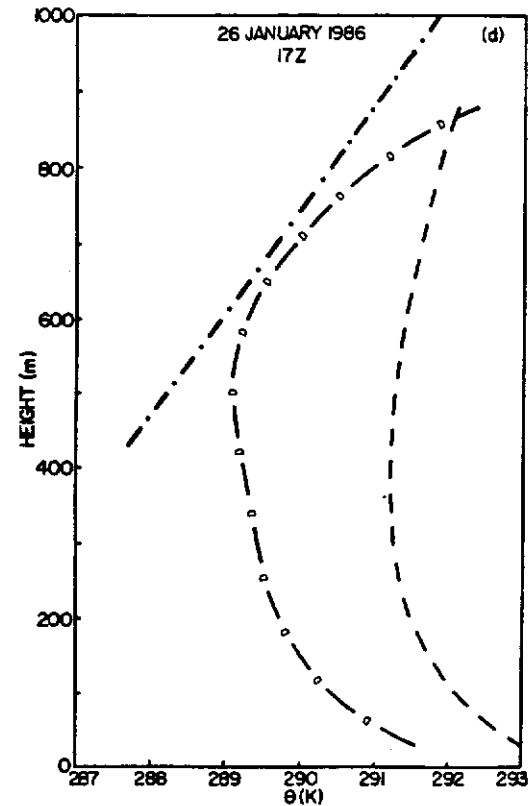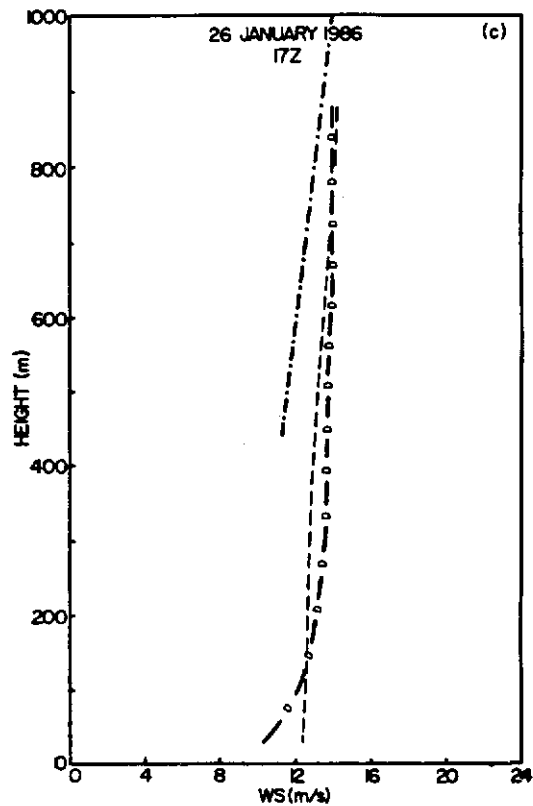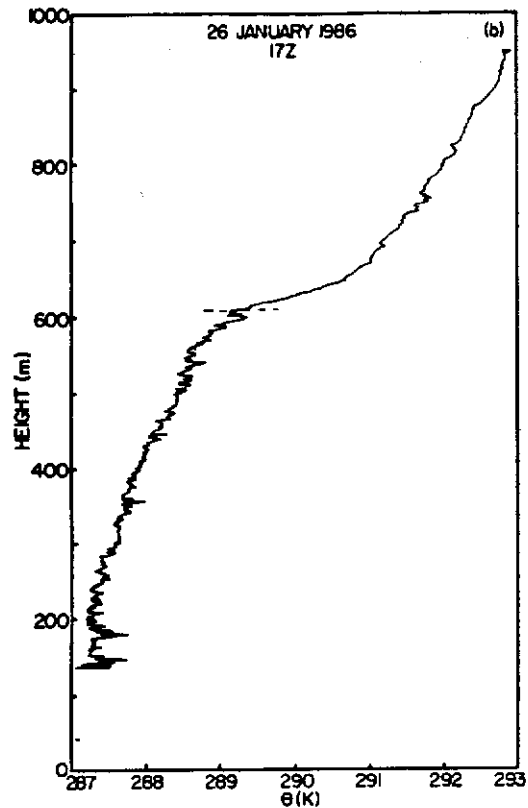2) The importance of properly parameterizing boundary layer mixing, especially in the convective
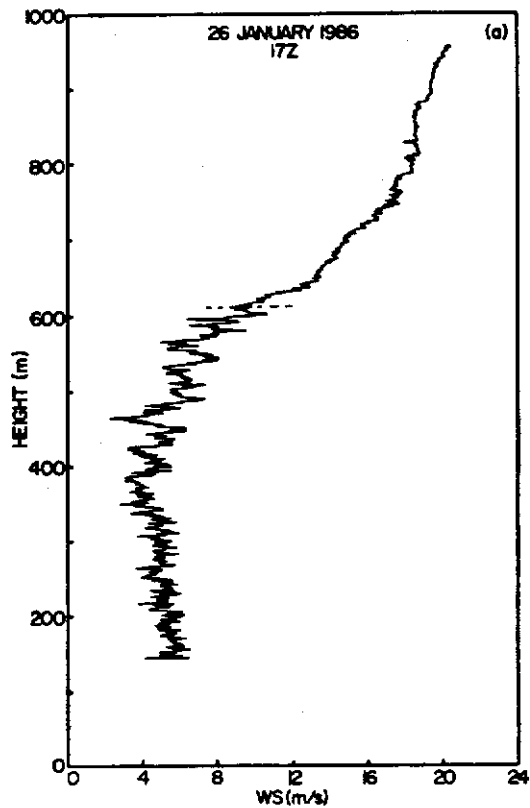
FIG. 19. Vertical ascent profiles obtained from the NCAR King Air at approximately 1700 UTC 26 January near 33.7°N, 77.0°W of (a) wind speed (m s⁻¹) and (b) potential temperature (K). The 29 h model simulations valid at 1700 UTC for model M10 (dot-dashed line), MB16 (dashed line) and EE16 (D-line) are also given for (c) wind speed and (d) potential temperature.

PBL, outweighs the importance of increased vertical model resolution. An increase in boundary layer resolution alone does not provide improvement in mesoscale structure for a less physically realistic parameterization of turbulent processes. For mixing-length parameterizations this emphasizes the need for stability dependence in the formulation of eddy viscosity profiles.

3) Model forecast skill based on S_1 scores shows little sensitivity in the larger mesoscale structure to changes in PBL parameterization. Similar skill scores are obtained regardless of the three PBL schemes tested. Thus, weaknesses evident in the smaller-scale analysis, such as the stability deficiency in model MB16, are not shown in the statistical results; however, cross-section and vertical profile analysis emphasize the need for a physically correct PBL parameterization, particularly on the mesoscale.

4) Sensitivity tests to surface latent and sensible heat fluxes emphasize their importance in the development of the coastal front system. Model simulations without fluxes show no coastal low pressure system and reduced precipitation.

5) 24 h model simulations with a TKE PBL parameterization generally show a stronger, more intense coastal front system. A deeper low pressure center is forecast as well as a stronger low-level jet, larger surface fluxes and a narrower and more intense ascent region along the front as compared to models with less complex PBL parameterizations.

6) Comparison to aircraft data obtained in the vicinity of the Gulf Stream approximately 5–6 h after the frontal passage supports the conclusions drawn from the model EE16 simulations of a deep, well-mixed postfrontal marine boundary layer.

Even in the comparison of high resolution GALE data, some of the results, such as the simulated low-level jet, are still not viable because horizontal model resolution exceeds state of the art observation networks. The need exists to rely on other types of observation systems such as ones involving wind profilers, Doppler radar and satellite technology. It must also be emphasized that numerical simulations are performed only for one case study, and results should not be expected to be totally representative for a wide variety of cases. In addition, it may not be desirable to emphasize one geographical point or location in the comparison of model simulations. Often the overall pattern is of more significance.

Further evaluation in the future involving more simulations of varying synoptic and mesoscale development should be considered. Further investigation is needed into the effects of boundary layer processes on stability changes in the moist baroclinic atmosphere. Future model studies to investigate the influence and sensitivity of latent heat release in the boundary layer on mesoscale systems are also needed.

REFERENCES

Akkarappuram, A. F., 1988: Air–sea exchange processes off the Carolinas during the 1986 East Coast winter storms-GALE (Genesis of Atlantic Lows Experiment). M.S. thesis, Department of Marine, Earth and Atmospheric Sciences, N.C. State University, Raleigh, NC 27695.

Anthes, R. A., 1977: A cumulus parameterization scheme utilizing a one-dimensional cloud model. *Mon. Wea. Rev.,* **105,** 270–286.

——, 1983: Regional models of the atmosphere in middle latitudes. *Mon. Wea. Rev.,* **111,** 1306–1335.

——, Y.-H. Kuo and J. R. Gyakum, 1983: Numerical simulations of a case of explosive marine cyclogenesis. *Mon. Wea. Rev.,* **111,** 1174–1188.

——, ——, E. Y. Hsie, S. Low-Nam and T. W. Bettge, 1989: Estimation of skill and uncertainty in regional numerical models. *Quart. J. Roy. Meteor. Soc.,* **115,** 763–806.

Arakawa, A., and V. R. Lamb, 1977: Computational design of the basic dynamical process of the UCLA general circulation model. *Methods Comput. Phys.,* **17,** 173–265.

Atkinson, B. W., 1981: *Mesoscale Atmospheric Circulations,* Academic Press, 495 pp.

Ballentine, R. J., 1980: A numerical investigation of New England coastal frontogenesis. *Mon. Wea. Rev.,* **108,** 1479–1497.

Blackadar, A. K., 1962: The vertical distribution of wind and turbulent exchanges in neutral atmosphere. *J. Geophys. Res.,* **67,** 3095–3102.

——, 1976: Modeling the nocturnal boundary layer. Preprints, *Third Symposium on Atmospheric Turbulence, Diffusion and Air Quality,* Raleigh, Amer. Meteor. Soc., 46–49.

Bond, N. A., and R. G. Fleagle, 1988: Prefrontal and postfrontal boundary layer processes over the ocean. *Mon. Wea. Rev.,* **116,** 1257–1273.

Bosart, L. F., 1975: New England coastal frontogenesis. *Quart. J. Roy. Meteor. Soc.,* **101,** 957–978.

——, 1981: The President's Day snowstorm of 18–19 February 1979: A subsynoptic scale event. *Mon. Wea. Rev.,* **109,** 1542–1566.

——, and S. C. Lin, 1984: A diagnostic analysis of the President's Day storm of February 1979. *Mon. Wea. Rev.,* **112,** 2148–2177.

Brehme, K. A., 1987: A method of objective analysis for meteorological fields for use in a numerical weather prediction model. M.S. thesis, Department of Marine, Earth and Atmospheric Sciences, N.C. State University, Raleigh, NC 27695.

Brost, R. A., J. C. Wyngaard and D. H. Lenschow, 1982: Marine stratocumulus layers. Part II: Turbulence budgets. *J. Atmos. Sci.,* **39,** 818–836.

Browning, K. A., M. E. Hardman, T. W. Harrold and C. W. Pardoe, 1973: The structure of rainbands within a midlatitude depression. *Quart. J. Roy. Meteor. Soc.,* **99,** 215–231.

——, F. F. Hill and C. W. Pardoe, 1974: Structure and mechanism of precipitation and the effect of orography in a winter time warm sector. *Quart. J. Roy. Meteor. Soc.,* **100,** 309–330.

Businger, J. A., J. C. Wyngaard, Y. Izumi and E. F. Bradley, 1971: Flux-profile relationship in the atmospheric surface layer. *J. Atmos. Sci.,* **28,** 181–189.

Chang, S. W., 1979: An efficient parameterization of convective and non-convective planetary boundary layers for use in numerical models. *J. Appl. Meteor.,* **18,** 1205–1215.

——, K. Brehme, R. Madala and K. Sashegyi, 1989: A numerical study of the East Coast snowstorm of 10–12 February 1983. *Mon. Wea. Rev.,* **117,** 1766–1776.

Chen, S.-J., and L. Dell'Osso, 1987: A numerical study of East Asian coastal cyclogenesis. *Mon. Wea. Rev.,* **115,** 477–487.

Chou, S.-H., D. Atlas and E.-N. Yeh, 1986: Turbulence in a convective marine atmospheric boundary layer. *J. Atmos. Sci.*, **43**, 547–564.

Danard, M. B., and G. E. Ellenton, 1980: Physical influences on East Coast cyclogenesis. *Atmosphere: Atmos.-Ocean*, **18**, 65–82.

Davies, H. C., and R. E. Turner, 1977: Updating prediction models by dynamical relaxation: An examination of the technique. *Quart. J. Roy. Meteor. Soc.*, **103**, 225–245.

Davis, C. A., and K. A. Emmanuel, 1988: Observational evidence for the influence of surface heat fluxes on rapid maritime cyclogenesis. *Mon. Wea. Rev.*, **116**, 2649–1659.

Detering, H. W., and D. Etling, 1985: Application of the $E - \epsilon$ turbulence model to the atmospheric boundary layer. *Bound.-Layer Meteor.*, **33**, 113–133.

Dirks, R. A., J. P. Kuettner and J. A. Moore, 1988: Genesis of Atlantic Lows Experiment (GALE): An overview. *Bull. Amer. Meteor. Soc.*, **69**, 148–160.

Fawcett, E. B., 1977: Current capabilities in prediction at the National Weather Service's National Meteorological Center. *Bull. Amer. Meteor. Soc.*, **58**, 143–149.

Friehe, C. A., and K. F. Schmitt, 1976: Parameterization of air–sea interface fluxes of sensible heat and moisture by the bulk aerodynamic formulas. *J. Phys. Oceanogr.*, **6**, 801–809.

Gerber, H., S. Chang and T. Holt, 1989: Evolution of a marine boundary layer jet. *J. Atmos. Sci.*, **46**, 1312–1326.

Holt, T., and S. Raman, 1988: A review and comparative evaluation of multi-level boundary layer parameterizations for first order and turbulent kinetic energy closure schemes. *Rev. Geophys.*, **26**, No. 4, 761–780.

—— and ——, 1990: Marine boundary layer structure and circulation in the region of offshore redevelopment of a cyclone during GALE, *Mon. Wea. Rev.*, **118**, 392–410.

Keyser, D., 1986: Atmospheric fronts: An observational perspective. *Mesoscale Meteorology and Forecasting*, P. S. Ray, Ed., Amer. Meteor. Soc., 216–258.

——, and R. A. Anthes, 1982: The influence of planetary boundary-layer physics of frontal structure in the Hoskins–Bretherton horizontal shear model. *J. Atmos. Sci.*, **39**, 1783–1802.

Kuo, H. L., 1974: Further studies of the parameterization of the influence of cumulus convection on large-scale flow. *J. Atmos. Sci.*, **31**, 1232–1240.

Kuo, Y.-H., and R. J. Reed, 1988: Numerical simulation of an explosively deepening cyclone in the Eastern Pacific. *Mon. Wea. Rev.*, **116**, 2081–2105.

Madala, R. V., S. W. Chang, U. C. Mohanty, S. C. Madan, R. K. Paliwal, V. B. Sarin, T. Holt and S. Raman, 1987: Description of Naval Research Laboratory limited area dynamical weather prediction model. NRL Technical Report 5992. [Available from NRL, Washington, D.C. 20375.]

Marks, F. D., and P. M. Austin, 1979: Effects of the New England coastal front on the distribution of precipitation. *Mon. Wea. Rev.*, **107**, 53–67.

Martin, D. W., B. Auvine and B. Hinton, 1988: Atlantic Ocean Satellite Rainmaps for GALE, CIMSS Report, April 1988. [Available from University of Wisconsin, Space Science Center, Madison, Wisconsin 53706.]

Monin, A. S., and A. M. Yaglom, 1971: *Statistical Fluid Mechanics, Vol. I*, MIT Press, 468–504.

Nuss, W. A., 1986: The influence of surface heat and moisture fluxes on explosive marine cyclogenesis. Ph.D. dissertation, Atmospheric Sciences Department, University of Washington, Seattle, WA 98195.

——, and R. A. Anthes, 1987: A numerical investigation of low-level processes in rapid cyclogenesis. *Mon. Wea. Rev.*, **115**, 2728–2743.

Ogura, Y., and D. Portis, 1982: Structure of the cold front observed in SESAME-AVE III and its comparison with the Hoskins–Bretherton frontogenesis model. *J. Atmos. Sci.*, **39**, 2773–2792.

Orlanski, I., 1975: A rational subdivision of scales for atmospheric processes. *Bull. Amer. Meteor. Soc.*, **56**, 527–530.

Perkey, D. J., and C. W. Kreitzberg, 1976: A time dependent lateral boundary scheme for limited-area primitive equation models. *Mon. Wea. Rev.*, **104**, 744–755.

Petterssen, S., D. L. Bradbury and K. Pederson, 1962: The Norwegian cyclone models in relation to heat and cold sources. *Geofys. Publ*, **24**, 243–280.

Raman, S., and A. J. Riordan, 1988: The Genesis of Atlantic Lows Experiment: The planetary–boundary-layer subprogram of GALE, *Bull. Amer. Meteor. Soc.*, **69**, 161–172.

Reynolds, R. W., 1982: Monthly averaged sea surface temperature climatology. NOAA Technical Report NWS-31. [Available from NOAA, Washington, D.C. 20233.]

Seller, W. D., 1965: *Physical Climatology*, University of Chicago Press, 53–54.

Shapiro, M. A., 1983: Mesoscale weather systems of the central United States, *The National STORM Program: Scientific and Technological Bases and Major Objectives*. R. A. Anthes, Ed., 3.1-3.77. [Available from University Corporation for Atmospheric Research, Boulder, CO, 80307.]

Uccellini, L. W., D. Keyser, K. F. Brill and C. H. Wash, 1985: The President's Day cyclone of 18–19 February 1979: Influence of upstream trough amplification and associated tropopause folding on rapid cyclogenesis. *Mon. Wea. Rev.*, **113**, 962–988.

Zhang, D., and R. A. Anthes, 1982: A high-resolution model of the planetary boundary layer-sensitivity tests and comparisons with SESAME-79 data. *J. Appl. Meteor.*, **21**, 1594–1609.